

# GeoMod 2014

## Modelling in Geosciences

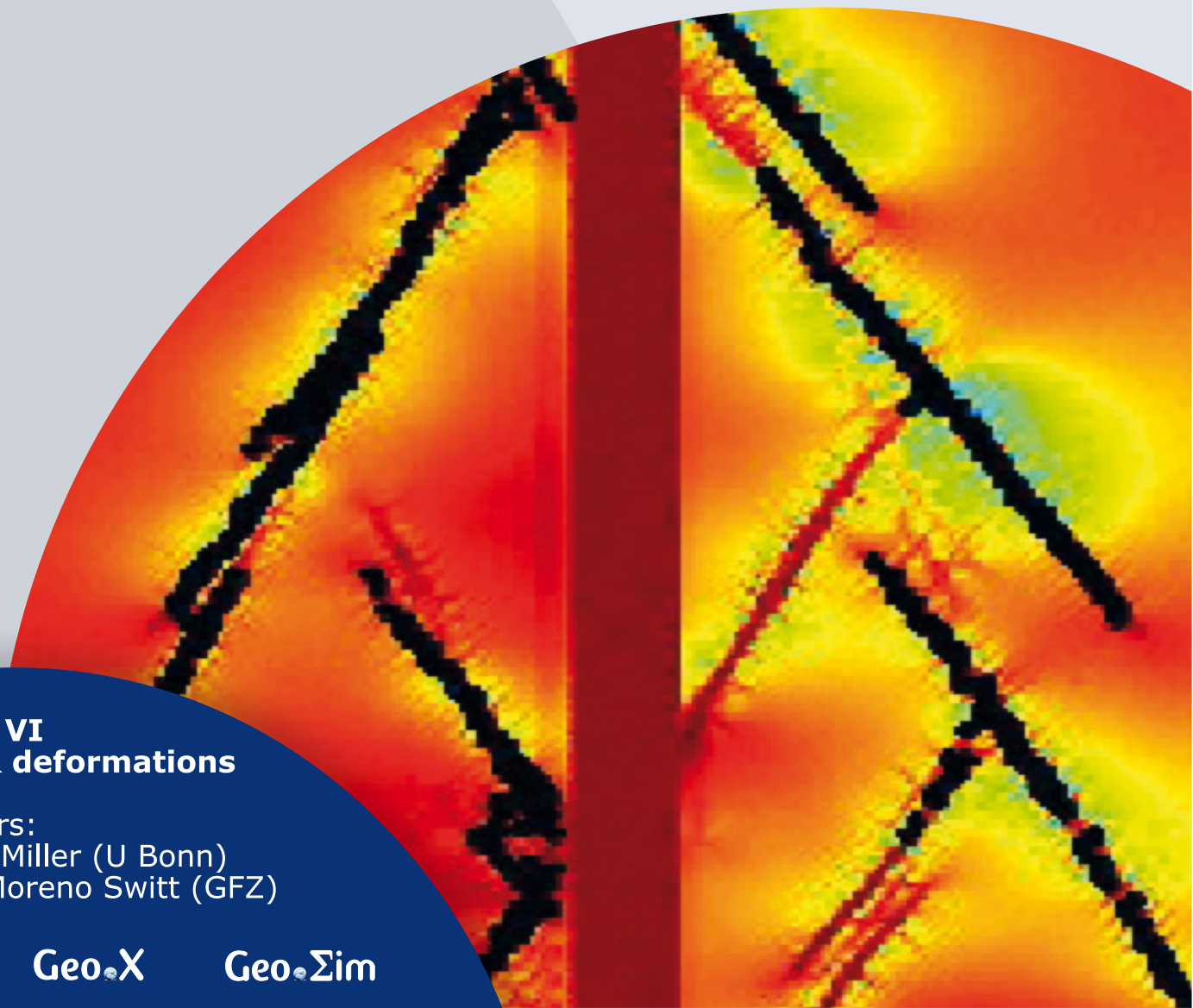
### Programme & Extended Abstracts

31 August - 5 September 2014

Editors:  
Kirsten Elger  
Øystein Thordén Haug  
Malte Ritter

#### Session VI Fluids & deformations

Conveners:  
Stephen Miller (U Bonn)  
Marcos Moreno Switt (GFZ)



## **Recommended Citation**

Elger, K; Haug, Ø. T.; Ritter, M. C. (Eds), (2014): Proceedings of GeoMod2014 – Modelling in Geosciences: Programme and Extended Abstracts 31 August–5 September 2014, GeoMod2014 – Modelling in Geosciences (Potsdam 2014), Potsdam: GFZ German Research Centre for Geosciences. DOI: <http://doi.org/10.2312/GFZ.geomod.2014.001>.

## **Disclaimer and Copyright**

Each author is responsible for the content of his or her abstract and has the copyright for his or her figures.

## **Imprint**

### **Publisher**

Helmholtz Centre Potsdam  
GFZ German Research Centre for Geosciences  
Telegrafenberg  
14473 Potsdam  
Published in Potsdam, Germany

### **Editors**

Kirsten Elger  
Øystein T. Haug  
Malte C. Ritter

doi: 10.2312/GFZ.geomod.2014.001

## About this book

This volume contains the extended abstracts of contributions presented during GeoMod 2014 at the Helmholtz Centre Potsdam GFZ German Research Centre for Geosciences (GFZ Potsdam), showing the state of the art of the tectonic modeling community.

GeoMod is a biennial conference dedicated to latest results of analogue and numerical modelling of lithospheric and mantle deformation. It started in 2002 in Milan as RealMod2002, then moved to Lucerne (GeoMod2004), Florence (2008), Lisbon (2010), and Lausanne (2012).

GeoMod2014 took place from 31 August to 3 September 2014 with 138 participants from 25 countries on all continents. The scientific programme of GeoMod2014 was organized in seven topical sessions listed below. The conference was followed by a 2-day short course on "Constitutive Laws: from Observation to Implementation in Models" (including lectures, lab visits, and practical exercises), as well as a 1-day hands-on tutorial on the ASPECT numerical modelling software.

GeoMod2014 focused on rheology and deformation at a wide range of temporal and spatial scales: from earthquakes to long-term deformation, from microstructures to orogens and subduction systems. For the first time, the discipline of volcanotectonics was included, while the (mantle) geodynamics community was more strongly represented than in previous editions. The bridge to field geology has traditionally been strong. At GeoMod 2014, fitting to the focus on rheology, the rock mechanics community was also represented. We thank our sponsors DFG, GFZ Potsdam and Geo.X, the conveners and all participants for contributing to a successful conference.

The GeoMod2014 Committee

## **The Scientific Committee**

Onno Oncken  
Georg Dresen  
Stephan Sobolev  
Matthias Rosenau  
Karen Leever

## **The Organising Committee**

Kirsten Elger  
Franziska Alberg  
Students support: Zahra Amirzada,  
Felix Eckelmann, Øystein Thordén Haug,  
Shaoyang Li, Malte Ritter, Tasca Santimano,  
Sarah Schröder, Johannes Wagner

## **Sessions, Conveners, and keynote speakers**

### **(Seismo-)tectonics**

*Conveners:* Boris Kaus (U Mainz), Onno Oncken (GFZ/FU Berlin),

*Keynotes:* Kelin Wang (Geological Survey Canada, Alberta), Bertrand Maillot (U Cergy-Pontoise)

### **Tectonics & Surface Processes**

*Conveners:* Fabien Graveleau (U Lille), Niels Hovius (GFZ/U Potsdam),

*Keynotes:* Ritske Huisman (U Bergen), Stéphane Dominguez (U Montpellier II)

### **Volcanism and Volcanotectonics**

*Conveners:* Olivier Galland (U Oslo), Eoghan Holohan (GFZ)

*Keynotes:* Rikke Pedersen (U Iceland), Olivier Roche (U BP Clermont-Ferrand)

### **Geodynamics**

*Conveners:* Francesca Funiciello (U Roma Tre), Stephan Sobolev (GFZ),

*Keynotes:* Anne Davaille (U Paris-Sud), Bernhard Steinberger (GFZ)

### **Rheology**

*Conveners:* Georg Dresen (GFZ/U Potsdam), Hiroki Sone (GFZ),

*Keynotes:* Yuri Fialko (U California), Laurent Montési (U Maryland)

### **Fluids and Deformation**

*Conveners:* Stephen Miller (U Bonn), Marcos Moreno Switt (GFZ),

*Keynotes:* Boris Galvan (U Bonn), Takeshi Tsuji (U Kyushu)

### **Methods and Materials (poster-only session)**

*Conveners:* Matthias Rosenau (GFZ), Marcel Frehner (ETH Zürich)

### **Short course on “Constitutive Laws: from Observation to Implementation in Models”**

*Lecturers:* Onno Oncken (GFZ Potsdam), Matthias Rosenau (GFZ Potsdam), Fabio Corbi (GFZ Potsdam), Georg Dresen (GFZ Potsdam), Stephan Sobolev (GFZ Potsdam), Sascha Brune (U Sydney)

### **Hands-on tutorial on “ASPECT: a next-generation geodynamic modelling software”**

(Advanced Solver for Problems in Earth’s ConvecTion)

*Lecturers:* Anne Glerum (Utrecht University), Juliane Dannberg (GFZ Potsdam). Supervised by Wolfgang Bangerth (Texas A&M University, ASPECT main developer), Stephan Sobolev (GFZ Potsdam), Bernhard Steinberger (GFZ Potsdam).

# Contents

<b>I. (Seismo-)tectonics</b>	<b>1</b>
<b>An investigation of seismicity and lithospheric features of the Zagros region, SW Iran, using coda wave attenuation</b> M. I. Ahmadzadeh, H. Rahimi, F. Sobouti	<b>3</b>
<b>Coseismic Coulomb stress changes on intra-continental normal and thrust faults: insights from three-dimensional finite-element modelling</b> M. Bagge, A. Hampel	<b>7</b>
<b>The role of pre-existing frictional weaknesses on the propagation of extensional fault</b> L. Bonini, R. Basili, P. Burrato, V. Kastelic, G. Toscani, S. Seno, G. Valensise	<b>9</b>
<b>Analogue models of subduction megathrust earthquakes: analyzing the viscoelastic rheological parameter space with an innovative monitoring technique</b> S. Brizzi, F. Corbi, F. Funicello, M. Moroni	<b>14</b>
<b>Upscaling of micro- and meso-scale structures to local- and regional scales: implications for 3D implicit and explicit models of structurally complex deformation of multi-layered rocks</b> M. Eggseder, A. Cruden	<b>17</b>
<b>Influence of the seismogenic downdip width on supercycles at subduction thrusts</b> R. Herrendörfer, Y. van Dinther, T. Gerya, L. A. Dalguer	<b>22</b>
<b>Geomechanical modeling of fault geometry role on subduction earthquake cycle: Case study of Chilean margin</b> S. Li, M. Moreno, J. Bedford, M. Rosenau, D. Melnick, O. Oncken	<b>26</b>
<b>The long term evolution of fold-and-thrust belts: consistency of numerical approaches and physical experiments</b> B. Maillot	<b>29</b>
<b>Cross-scale model of seismic cycle: first results</b> I. A. Muldashev, S. V. Sobolev	<b>33</b>
<b>Numerical modelling of the instantaneous subduction dynamics of the Banda Arc region</b> C. Pranger, C. Thieulot, A. van den Berg, W. Spakman	<b>36</b>
<b>Towards 3D seismo-thermo-mechanical models of the subduction thrust</b> C. Pranger, Y. van Dinther, T. Gerya, F. Corbi, F. Funicello	<b>37</b>

<b>Smart or Beautiful? Accretionary wedge evolution seen as a competition between minimum work and critical taper</b>	
T. Santimano, M. Rosenau, O. Oncken	39
<b>CHANDRAYAAN-1 data infers tectonic activity on the south pole of the moon</b>	
P. Singh, S. Mukherjee	43
<b>The concepts of complex network advance understanding of earthquake science</b>	
N. Suzuki	46
<b>Hypothesis of geodynamic processes in the lithosphere under catastrophic earthquake Tohoku-Oki</b>	
V. N. Tatarinov, A. I. Kagan, T. A. Tatarinova	49
<b>Seismo-thermo-mechanical modeling of subduction zone seismicity</b>	
Y. van Dinther, T. Gerya, L. A. Dalguer, P. M. Mai	52
<b>Thermal Expressions of Stick-slip and Creeping Subduction Megathrusts</b>	
K. Wang, X. Gao	56
<b>II. Tectonics and Surface Processes</b>	<b>60</b>
<b>Neotectonic evolution of the El Salvador Fault Zone. Insights from 4D analogue experiments.</b>	
J. Alonso-Henar, G. Schreurs, J.J. Martínez-Díaz, J.A. Álvarez-Gómez	62
<b>Restraining and releasing bands along a sinistral strike-slip shear zone: A physical modeling approach</b>	
A. Blanco, F. C. Alves da Silva	67
<b>Numerical basin modelling of a salt rim syncline: insights into rim syncline evolution and salt diapirism</b>	
C. Brandes, J. Winsemann	71
<b>Modelling Syntectonic Sedimentation in a Extensional Faults System</b>	
A. Carmona, R. Clavera-Gispert, O. Gratacós, S. Hardy, J. A. M. de la Fuente	75
<b>Process-Based Forward Numerical Modelling SIMSAFADIM-CLASTIC: The Vilomara Composite Sequence case (Eocene, Ebro basin, NE Iberian Peninsula).</b>	
R. Clavera-Gispert, O. Gratacós, M. López-Blanco, R. Tolosana-Delgado	80
<b>The balance between uplift and fluvial erosion over a single seismic cycle – an example from Taiwan</b>	
K. Cook, F. Graveleau, J. Turowski, N. Hovius. J. Suppe	84
<b>Joint analog modeling of marine and terrestrial geological processes: state of the art and new developments</b>	
S. Dominguez	85

<b>Fold growth rates in 3D buckle folds</b>	<b>89</b>
M.Frehner	
<b>Furrow-and-ridge morphology on rockglaciers explained by gravity-driven buckle folding: A case study from the Murtèl rockglacier (Switzerland)</b>	<b>95</b>
M. Frehner, I. Gärtner-Roer, A. H. M. Ling	
<b>Structural evolution and structural style of South Eastern Kohat deciphered through 3D geoseismic model using MOVE software, Shakardarra area, KP Pakistan</b>	<b>101</b>
H. Ghani, H. Hussain, M. Zafar, I. Khan, A. Malik, M. Abid, E. Javed	
<b>Lithospheric scale analogue models of the southern Gulf of California oblique rift</b>	<b>108</b>
D. Gracia-Marroquín, R. Portillo-Pineda, M. Cerca, G. Corti	
<b>The negative inversion of thrust faults and related basin geometries: insight from analogue modelling experiments</b>	<b>112</b>
F. Graveleau, O. Averbuch, B. Vendeville, A. Quinon, M. Ouzgaït	
<b>Experimental modelling of deformation-erosion-sedimentation interactions in compressional, extensional and strike-slip settings</b>	<b>114</b>
F. Graveleau, V. Strak, S. Dominguez, J. Malavieille, M. Chatton, I. Manighetti, C. Petit	
<b>Linking lithosphere deformation and sedimentary basin formation over multiple scales</b>	<b>116</b>
R. S. Huismans	
<b>3D Analogue Modelling of the Effect of Fan Sedimentation on Accretionary Wedge Dynamics – the Magdalena Fan case, South Caribbean Margin, Colombia</b>	<b>117</b>
K. Leever, E. Johansen	
<b>From continental rifting to seafloor spreading: Insight from 3D thermo-mechanical modeling</b>	<b>121</b>
J. Liao, T. Gerya	
<b>Dynamic Modelling of Accretionary Prisms and Stratigraphy of Forearc basins</b>	<b>131</b>
U. Mannu, K. Ueda, S. D. Willett, T. Gerya, M. Strasser	
<b>Evolution of topography of post-Devonian Scandinavia: Effects and rates of erosion</b>	<b>136</b>
S. Medvedev, E. H. Hartz	
<b>Numerical modeling of main inverted structures in the Western Barents Sea.</b>	<b>140</b>
M. A. F. Miraj, C. Pascal, R. H. Gabrielsen, J. I. Faleide	
<b>Exploratory analog modeling of the effects of a morpho-rheological obstacle across a wrench fault system: the example of the Gloria Fault – Tore Madeira Rise intersection in NE Atlantic</b>	<b>144</b>
F. M. Rosas, J. Almeida, F. Barata, B. Carvalho, P. Terrinha, J. Duarte, C. Kullberg, R. Tomás	
<b>DANSER: an open source surface evolution code beyond coupling with tectonic models</b>	<b>149</b>
S. Schroeder, R. Gloaguen, J. Tjympel, A. Babeyko, S. V. Sobolev	

<b>Kinematic reconstruction of the Hastings block, southern New England Orogen, Australia</b> J. Yan, P. Lennox, B. F. J. Kelly, R. Offler	<b>153</b>
<b>Stability of over-pressured cohesive and frictional materials based on Sequential Limit Analysis</b> X. Yuan, Y. M. Leroy, B. Maillot, Y. Guéguen	<b>159</b>
<b>4D Transfer Zone Modeling in Continental Rifts</b> F. Zwaan, G. Schreurs	<b>164</b>
<b>III. Volcanism and Volcanotectonics</b>	<b>170</b>
<b>Solidification effects on sill formation: an experimental approach</b> L. Chaneaux, T. Menand	<b>172</b>
<b>The origin of circumferential fissures: insights from analog models</b> F. Corbi, E. Rivalta, V. Pinel, F. Maccaferri, V. Acocella	<b>177</b>
<b>Megatsunami generation from caldera subsidence</b> B. Kennedy, M. Gallagher, C. Gomez, T. Davies	<b>178</b>
<b>Toward a unified dynamic model for dikes and cone sheets in volcanic systems</b> O. Galland, S. Burchardt, E. Hallot, R. Mourgues, C. Bulois	<b>181</b>
<b>Morphology and dynamics of explosive vents through cohesive rock formations</b> O. Galland, G. Gisler, Ø. T. Haug	<b>185</b>
<b>Temporal changes in mantle wedge geometry and magma generation processes in the Central Andes: towards linking petrological data to thermomechanical models</b> R. Heistek, M. Brandmeier, H. Freymuth, G. Wörner	<b>188</b>
<b>Use of the Distinct Element Method in Volcano-tectonic Modeling</b> E. P. Holohan, H. Sudhaus, M. P. J. Schöpfer, T. R. Walter, J. J. Walsh	<b>191</b>
<b>Three-Dimensional Analysis of dike/fault interaction at Mono Basin (California) using the Finite Element Method</b> D. La Marra, M. Battaglia	<b>196</b>
<b>Modeling of Cooling History for the Jurassic Composite Granitic Plutons in the Central Nanling Region, South China: Implications for the Mineralization Process and Tectonic Evolution</b> H. Li, K. Watanabe, K. Yonezu	<b>201</b>
<b>The gravitational unloading due to rift depression: A mechanism for the formation of off-rift volcanoes in (continental) rift zones</b> F. Maccaferri, E. Rivalta, D. Keir, V. Acocella	<b>206</b>



<b>The formation of terrace-bounding faults on Olympus Mons volcano, Mars</b>	
S. Musiol, B. Cailleau, E. P. Holohan, T. R. Walter, D. A. Williams, A. Dumke, S. van Gasselt	211
<b>Surface deformation simulations of volcanic and tectonic processes in Iceland</b>	
R. Pedersen	214
<b>Overburden bulking in analogue models of depletion-induced collapse quantified with computed X-ray micro-tomography</b>	
S. Poppe, E. P. Holohan, E. Pauwels, V. Chudde, M. Kervyn	217
<b>Mechanisms of entrainment of a granular substrate by pyroclastic density currents: insights from laboratory experiments and models, and implications for flow dynamics.</b>	
O. Roche, Y. Niño	221
<b>Influence of crust type on the long-term deformation of a volcano: example from Mt. Etna (Italy)</b>	
S. Scudero, G. De Guidi, S. Imposa, M. Palano	226
<b>Analogue and numerical modeling of rifting events. Complementary tools to understand the rifting process.</b>	
D. Tripanera, D. Lamarra, V. Acocella, J. Ruch, E. Rivalta	231
<b>IV. Geodynamics</b>	<b>233</b>
<b>Anomalous structure of the oceanic lithosphere in the North Atlantic and Arctic oceans: preliminary analysis based on bathymetry, gravity and crustal structure</b>	
O. Barantseva, I. M. Artemieva, H. Thybo, M. Herceg	235
<b>Constraining the rheology of the lithosphere through geodynamic inverse modelling</b>	
T. Baumann, B. Kaus, A. Popov	237
<b>A new model for the architecture of magma-poor rifted margins</b>	
S. Brune, C. Heine, M. Pérez-Gussinyé, S. V. Sobolev	239
<b>Oblique extensional structures from initial deformation to breakup: Insights from numerical 3D lithospheric-scale experiments</b>	
S. Brune	242
<b>Initial models of the influence of collision-phase inheritance on continental rifting</b>	
S. Buitter, J. Tetreault, R. Ghazian	246
<b>Modelling subsidence history of rift-type basins</b>	
M. Cacace, M. Scheck-Wenderoth	247
<b>Strain localization during compression of a laterally heterogeneous lithosphere</b>	
E. Calignano, D. Sokoutis, E. Willingshofer	249

<b>3-D numerical modeling of subduction evolution of the western Mediterranean region</b>	
M. V. Chertova, W. Spakman, A. P. van den Berg, T. Geenen, D. J. J. van Hinsbergen	254
<b>Surface manifestations of low-buoyancy mantle plumes: Insights from geodynamic modeling</b>	
J. Dannberg, S. V. Sobolev	259
<b>Plumes to plate tectonics: insights from laboratory experiments</b>	
A. Davaille	261
<b>Three dimensional laboratory models of subduction: plate interface, overriding plate deformation and energy dissipation</b>	
J. C. Duarte, Z. Chen, W. P. Schellart, A. R. Cruden	266
<b>Geometrical transitions of mantle plumes: an insight from numerical simulations</b>	
U. Dutta, S. Sarkar, N. Mandal	269
<b>Thermo-mechanically coupled subduction with a free surface using ASPECT</b>	
M. Fraters, A. Glerum, C. Thieulot, W. Spakman	272
<b>The Role of the Initial Condition in Numerical Models of the Present-day Mantle Flow Field</b>	
E. H. Fritzell, A. L. Aller, G. E. Shephard	275
<b>3-D computational modeling of the continental plate collision near South Island, New Zealand</b>	
L. Karatun, C. Thieulot, R. Pysklywec	276
<b>Featuring lithosphere rheology in models of glacial isostatic adjustment</b>	
V. Klemann, M. Tesauro, Z. Martinec, I. Sasgen	278
<b>The 3D density and temperature distribution in an intracratonic basin setting: The Barents Sea and Kara Sea region</b>	
P. Klitzke, J. I. Faleide, J. Sippel, M. Scheck-Wenderoth	281
<b>The effect of melting and crustal production on plate tectonics on terrestrial planets</b>	
D. L. Lourenço, P. J. Tackley	284
<b>3-D numerical modelling of subduction initiation at curved passive margins</b>	
F. O. Marques, F. R. Cabral, T. V. Gerya, G. Zhu, D. A. May	285
<b>Crustal deformation and magmatism at the transition between subduction and collisional domains: insight from 3D numerical modeling</b>	
A. Menant, P. Sternai, L. Jolivet, L. Guillou-Frottier, T. Gerya	289
<b>Segregation, Accumulation, and Entrainment of the Oceanic Crust in the Lowermost Mantle: Exploring the Range of Governing Parameters with Numerical Modelling</b>	
E. Mulyukova, B. Steinberger, M. Dabrowski, S. V. Sobolev	294
<b>Role of extensional strain-rate on lithosphere necking architecture during continental rifting</b>	
Y. Nestola, F. Storti, C. CavoZZi	298

<b>Toroidal, counter-toroidal, and poloidal flows of the Rivera and Cocos plates</b> F. Neumann, A Vazquez, G Tolson, J. Contreras	<b>299</b>
<b>Estimating Crustal Thickness of Iran Using Euler Deconvolution Method and EIGEN-GL04C Geopotential Model</b> S. Parang	<b>300</b>
<b>How do weak plate boundaries affect the dynamic topography and geoid?</b> A. G. Petrunin, M. K. Kaban, B. Steinberger, H. Schmeling	<b>304</b>
<b>The development of topographic plateaus in an India-Asia-like collision zone using 3D numerical simulations</b> A. E. Pusok, B. Kaus, A. Popov	<b>308</b>
<b>Towards quantification of the interplay between strain weakening and strain localisation using analogue models</b> M. C. Ritter, M. Rosenau, K. Leever, O. Oncken	<b>310</b>
<b>Modelling plate kinematics, slabs and LLSVP dynamics – an example from the Arctic and northern Panthalassa</b> G. E. Shephard, A. L. Bull, C. Gaina	<b>313</b>
<b>Strike-slip movements and Rotation of tectonic blocks in the Kaboodan area, south Khur, Central Iran</b> A. Sohrabi, A. Nadimi	<b>318</b>
<b>On the relation between plate tectonics, large-scale mantle flow and mantle plumes: Some recent results and many open questions</b> B. Steinberger, R. Gassmoeller, E. Mulyukova, J. Dannberg, S. V. Sobolev	<b>320</b>
<b>The role of crustal thickness and lithospheric rheology on rifted margins width and tectonic subsidence</b> A. E. Svartman Dias, L. L. Lavier, N. W. Hayman	<b>324</b>
<b>Influence of Melting on the Long-Term Thermo-Chemical Evolution of Earth's Deep Mantle</b> P. J. Tackley, D. Lourenço, I. Fomin, T. Nakagawa	<b>329</b>
<b>A two- and three-dimensional numerical modelling benchmark of slab detachment</b> C. Thieulot, A. Glerum, B. Hillebrand, S. Schmalholz, W. Spakman, T. Torsvik	<b>331</b>
<b>The effect of strong heterogeneities in the upper mantle rheology on the dynamic topography and geoid</b> A. O. Tutu	<b>332</b>
<b>The role of weak seeds in numerical modelling of continental extensional systems</b> I. van Zelst, C. Thieulot, S. J. H. Buiters, J. Naliboff, W. Spakman	<b>334</b>

<b>The up side down logic of orogenic collision: on the formation of low-topography mountain ranges</b>	
K. Vogt, L. Matenco, T. Geyra, S. Gloetingh	336
<b>Implementing fluid flow in SLIM-3D</b>	
M. Walter, J. Quinteros, S. V. Sobolev	340
<b>The mechanical erosion of refertilized continental lithosphere by plume driven mantle flow</b>	
H. Wang, J. van Hunen, D. G. Pearson	342
<b>Deformation of forearcs during ridge subduction</b>	
S. Zeumann, A. Hampel	347
<b>V. Rheology</b>	<b>350</b>
<b>Fold Geometry Toolbox 2: A New Tool to Estimate Mechanical Parameters and Shortening from Fold Geometry</b>	
M. Adamuszek, M. Dabrowski, D. W. Schmid	352
<b>Mechanical anisotropy development and localization in two-phase composite rocks.</b>	
M. Dabrowski	355
<b>Numerical models of ductile roots of mature strike-slip faults</b>	
Y. Fialko	358
<b>Present-day intra-plate deformation of the Eurasian plate</b>	
C. Garcia-Sancho, R. Gover, K. N. Warners-Ruckstuhl, M. Tesauero	363
<b>Localization of deformation in a polymineralic material</b>	
S. Jammes, L. L. Lavier, J. E. Reber	365
<b>Localization processes on Earth, Mars, and Venus</b>	
L. G. J. Montési, F. Gueydan	368
<b>Rheology of bubble- and crystal-bearing magma: new analogue experimental data and an effective-medium model</b>	
S. P. Mueller, J. M. Truby, E. W. Llewellyn, H. M. Mader	372
<b>Modeling stress evolution around a rising salt diapir</b>	
M. A. Nikolinakou, P. B. Flemings, M. R. Hudec	376
<b>Numerical bifurcation analysis of spontaneous strain localization resulting in necking of a layer</b>	
M. Peters, T. Poulet, M. Veveakis, A. Karrech, M. Herwegh, K. Regenauer-Lieb	381
<b>Finite element model investigation of fault shear stress accumulation due to elastic loading and viscous relaxation.</b>	
H. Sone	385

<b>Lithospheric strength and elastic thickness variations in the North American continent</b> M. Tesauero, M. K. Kaban, S. Cloetingh, W. D. Mooney	<b>387</b>
<b>VI. Fluids and Deformation</b>	<b>391</b>
<b>Effect of Fluid Circulation on Intermediate-Depths Subduction Dynamics: From Field Observations to Numerical Modelling</b> S. Angiboust, S. Wolf, E. Burov, P. Agard, P. Yamato	<b>393</b>
<b>Assessment of microbial contamination of groundwater near solid waste dumpsites in basement complex formation, using total plate count method</b> B. S. Badmus	<b>395</b>
<b>Physico-chemical properties of soil samples and environmental impact of dumpsite on groundwater quality in basement complex terrain, south western Nigeria</b> B. S. Badmus	<b>396</b>
<b>Towards a general simulation tool for complex fluid-rock lithospheric processes: merging pre-processing, processing and post-processing in state-of-the-art computational devices</b> B. Galvan, S. Hamidi, T. Heinze, M. Khatami, G. Jansen, S. Miller	<b>397</b>
<b>THC modelling of an Enhanced Geothermal System</b> S. Hamidi, T. Heinze, B. Galvan, S. Miller,	<b>401</b>
<b>Numerical Modelling of earthquake swarms in the Vogtland / West-Bohemia</b> T. Heinze, S. Hamidi, B. Galvan, S. Miller	<b>404</b>
<b>Modelling of fractured reservoirs: fluid-rock interactions within fault domains</b> A. Jacquey, M. Cacace, G. Blöcher, M. Scheck-Wenderoth	<b>407</b>
<b>Heat transport mechanisms at different scales – a 3D modelling workflow</b> M. Scheck-Wenderoth, M. Cacace, J. Sippel, Y. Petrovich Maystrenko, Y. Cherubini, V. Noack, B. Onno Kaiser, B. Lewerenz	<b>412</b>
<b>Digital rock physics: Insight into fluid flow and elastic deformation of porous media</b> T. Tsuji	<b>417</b>
<b>VII. Methods and Materials</b>	<b>422</b>
<b>Seismological monitoring of lab-scale landslides: Method &amp; bouncing ball benchmark</b> Z. Amirzada, Ø. T. Haug, A. Burtin, T. Eken, M. Rosenau	<b>424</b>
<b>Small-scale modelling of ice flow perturbations induced by sudden ice shelf breakup</b> G. Corti, A. Zeoli, I. Iandelli	<b>428</b>
<b>Carbopol® for experimental tectonics: a rheological benchmark study</b> E. Di Giuseppe, F. Corbi, F. Funicello, A. Massmeyer, T.N. Santimano	<b>430</b>

<b>Initiation process of the frontal thrust revealed from detailed analogue experiments</b>	<b>434</b>
T. Dotare, Y. Yamada, T. Hori, H. Sakaguchi	
<b>The Use of Scaling Theory in Geological Laboratory Models</b>	<b>439</b>
O. Galland, E. Holohan, G. Dumazer	
<b>Testing tools for the generation of an unstructured tetrahedral grid on a realistic 3D underground model</b>	<b>443</b>
I. Görz, F. Träger, B. Zehner, J. Pellerin	
<b>Flanking structures – New insights from analogue models</b>	<b>448</b>
C. J. S. Gomes, B. A. Rodrigues, I. Endo	
<b>The Ribbon Tool</b>	<b>452</b>
J. Großmann, J. F. Ellis, H. Broichhausen	
<b>A new method to study the energy budget of rock fragmentation</b>	<b>457</b>
Ø. T. Haug, M. Rosenau, Z. Amirzada, K. Leever, O. Oncken	
<b>Fringes projection for 3D displacement analysis of experimental dry granular avalanches</b>	<b>459</b>
C. Mares, B. Barrientos-García, M. Cerca, D. Sarocchi, L. A. R. Sedano	
<b>A 3-D Lagrangian finite element algorithm with contour-based re-meshing for simulating large-strain hydrodynamic instabilities in visco-elastic fluids</b>	<b>464</b>
M. von Tscharnier, S. Schmalholz	
<b>Some Remarks on wet gypsum as a viscous material for physical modeling</b>	<b>467</b>
A. Yassaghi	
<b>Scientific Programme</b>	<b>471</b>
<b>Short Course Programme</b>	<b>475</b>

**Session VI.**

**Fluids and Deformation**

## **Session Description: Fluids and Deformations**

**Conveners: Stephen Miller (U Bonn), Marcos Moreno Switt (GFZ)**

This session is focused on the interactions between elastic and inelastic deformation, brittle failure (earthquakes), how fluids affect and are affected by, coupled deformation, as well as the importance of flow for numerous geodynamic processes. These include, but are not limited to, non-volcanic tremor and slow-slip earthquakes, enhanced geothermal systems, post-seismic deformation, earthquake swarms, and aftershocks. Although the interactions between fluids and deformation are conceptually straightforward, complexity arises due to multiple feedbacks between crack nucleation, growth, and coalescence combined with the initiation of fluid flow and an evolving pore-elastic/ fracture stress state. Modeling these processes is numerically challenging because the underlying physics require high-resolution simulations over a wide range of timescales. This session aims to understand fluids and deformation of a wide range of space and time scales, using recent advances in numerical modeling to compare with observations from experimentalists, geodesists, and geologists.



# Effect of Fluid Circulation on Intermediate-Depths Subduction Dynamics: From Field Observations to Numerical Modelling

S. Angiboust<sup>1,2</sup>, S. Wolf<sup>1</sup>, E. Burov<sup>1</sup>, P. Agard<sup>1</sup>, P. Yamato<sup>3</sup>

<sup>1</sup>*ISTeP, Univ. P.M. Curie-Paris 6, Paris, France*

<sup>2</sup>*Lithosphere dynamics laboratory, GFZ Potsdam, Germany*

<sup>3</sup>*Laboratoire de Tectonique, Univ. Rennes 1, France*

*e-mail: samuel.angiboust@gfz-potsdam.de*

*session: Fluids and Deformation*

A wide range of geophysical/petrological data indicates that large amounts of water are released in subduction zones during the burial of oceanic lithosphere through metamorphism and associated dehydration reactions. Large volumes of aqueous fluids are expected and observed in the mantle wedge, just below the continental Moho. Recent estimates suggest that the mantle wedge is heterogeneously serpentized (generally 20-30%). This serpentization is believed to cause a significant weakening of the mantle wedge and therefore may critically control the depth of interplate seismogenic coupling. However, data constraining mechanisms driving deep (50 km to 200 km) fluid circulation are lacking and fluid-rock interaction processes remain weakly constrained at the km-scale.

We herein propose a new fluid migration algorithm based on field relationships and thermodynamic modelling (PerpleX) where fluids are free to migrate, driven by rock fluid concentration, non-lithostatic pressure gradients and deformation. Oceanic subduction is then modelled using a forward visco-elasto-plastic thermomechanical code (FLAMAR algorithm) in which fluid transport and rheological effect is implemented. After 15 Ma of convergence between the two plates, we show that deformation is accommodated along a low-strength shear zone in the wall of the subduction thrust interface, characterized by a weak (10-25 % serp.) and relatively narrow (between

3 km to 6 km) serpentized front/channel.

Our results also show that dehydration associated with eclogitization of oceanic crust (60 km to 75 km and serpentinite breakdown (110 km to 130 km) significantly weakens the mantle wedge at these depths, thereby favoring underplating of oceanic plate material in the deep mantle wedge (Angiboust et al., 2012). Hydration of the subduction interface also significantly weakens the interface and enables detachment and stacking of slices from the downgoing slab. We finally show that modelled geometries are in good agreement with reconstructions derived from field structural observations made along the Western Alps eclogite-facies ophiolitic belt, where large, coherent slices were detached at c. 80 km depth in the Alpine subduction zone (Fig. 1).

## References

Angiboust, S., Wolf, S., Burov, E., Agard, P., & Yamato, P. (2012). Effect of fluid circulation on subduction interface tectonic processes: Insights from thermo-mechanical numerical modelling. *Earth and Planetary Science Letters*, 357, 238-248.

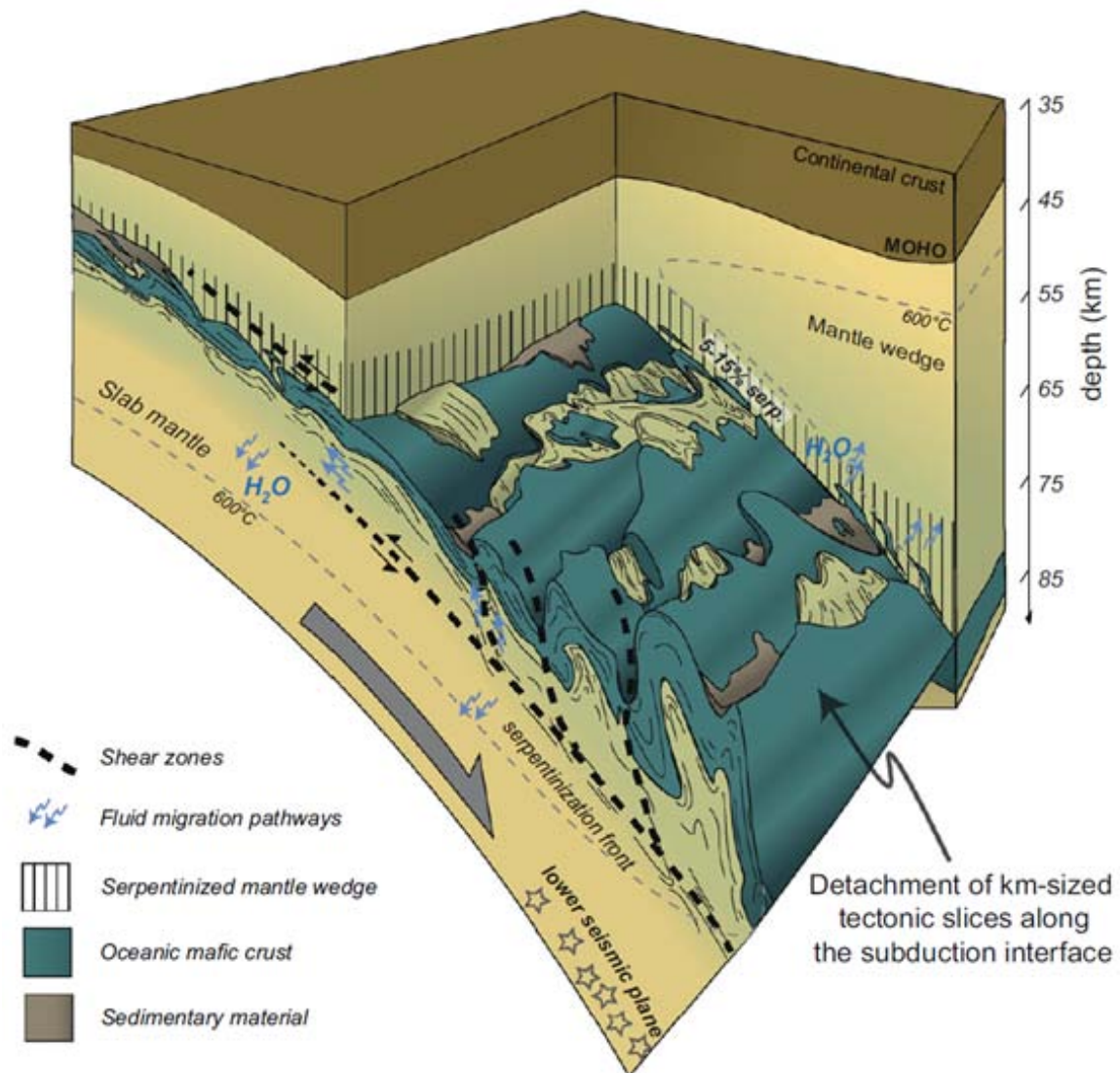


Fig. 1.: Schematic view drawn from field and numerical modeling results of the subduction interface region showing the detachment of large slices of oceanic lithosphere between 60 km and 80 km depths (Angiboust et al., 2012).

# **Assessment of microbial contamination of groundwater near solid waste dumpsites in basement complex formation, using total plate count method**

Biodun Suraj Badmus

*Federal University of Agriculture Abeokuta*

*e-mail: badmusbs@yahoo.co.uk*

*session: Fluids and Deformation*

## **Abstract**

Microbial analysis of water samples collected from two selected dumpsites within Ibadan metropolis were carried out in order to ascertain the effects of leachates generated by dumpsite on groundwater quality. Water samples were collected from surrounding wells and stream near Aba-Eku and Ajakanga solid waste landfill in Southwestern part of Nigeria. The samples were analysed for coliform count and Escherichia Coli through total plate count method. The result of the microbial analysis reveals high presence of coliform in all the water samples while two wells around Aba Eku dumpsite have E. Coli presence and none is detected in wells and stream around Ajakanga landfill. High values of microbial counts are principal indicators of suitability of water for domestic purpose and also sign of groundwater contamination in the surrounding wells. The sign of groundwater contamination was noticed in many surrounding wells around the two dumpsites resulting in high number of coliform bacteria. The presence of E. coli in wells 2 and 7 in Aba Eku requires control measures before consumption.

# Physico-chemical properties of soil samples and environmental impact of dumpsite on groundwater quality in basement complex terrain, south western Nigeria

Biodun Suraj Badmus

*Federal University of Agriculture Abeokuta*

*e-mail: badmusbs@yahoo.co.uk*

*session: Fluids and Deformation*

## Abstract

Physiochemical and microbial analyses of water samples from hand-dug wells were carried out around active dumpsite and or soil samples to ascertain the effect of wastes on the groundwater and soil quality. Soil samples were collected up to depth of 100 cm with the aid of soil auger while water samples were collected inside a 2 L PVC bottle. Soil pH, EC, % OM, % OC values ranged from 5.45–6.45, 5.03–6.63, 2.39–9.14 and 1.39–5.30. The mean values of soil pH, EC, % OM, % OC are high when compared with control. For water samples, the parameters of interest for microbial analysis are: coliform count and *E. coli* while parameters determined for physio-chemical analysis are: pH, Total Dissolved Solid (TDS), Electrical Conductivity (EC), Hardness, Carbonate, Bicarbonate, Chloride, Nitrate, Sulphate, Calcium, Magnesium, Potassium and Sodium ions. Microbial analysis revealed severe pollution in all samples while most of physiochemical parameters indicated traceable pollution which were below the World Health Organization (WHO) standard for human consumption as well as the Nigerian Standard for Drinking Water Quality (NSDWQ) limits. However, Well 5 which is close to the landfill has high values for all analyzed parameters when compared with other wells.

# Towards a general simulation tool for complex fluid-rock lithospheric processes: merging pre-processing, processing and post-processing in state-of-the-art computational devices

Boris Galvan, Sahar Hamidi, Thomas Heinze, Mohammad Khatami, Gunnar Jansen, Stephen Miller

*Geodynamics/Geophysics, University of Bonn*

*e-mail: galvan@geo.uni-bonn.de*

*session: Fluids and Deformation*

Study of flow through porous and fractured media is a very active research area, with many different models and numerical tools available. Most of these tools are designed to study coupled processes of fluid flow, heat flow, and chemistry, and results from these models have proven valid in many real world applications.

However, the development of new engineering techniques requires new tools to address more complex scenarios. For example, fracking, enhanced geothermal systems, and CO<sub>2</sub> /gas sequestration and storage play a very important role in the world's energy and environmental requirements. This tendency will likely steeply increase in the future.

The principle problem for the general applicability of all these techniques relates to uncontrolled and unexpected effects of fluid-triggered rock deformation. For example, induced seismicity can disturb the population, with possible infrastructure damage or unplanned flow paths that may lead to aquifers and soil pollution.

Therefore, there is need for new tools that consider the full coupling between rock deformation and fluid flow that use state-of-the-art fluid flow and rock deformation models. Desired fluid flow models should include saturated and unsaturated porous media and multiphase-multicomponent flow with local and nonlocal thermal equilibrium.

They are few tools available that are capable of solving such models and, to the best of our knowledge, none of these models include the case for non-local thermal equilibrium. Such models are necessary to address real world problems like the stimulation stages in enhanced geothermal systems or fracking (Figure 1).

Rock deformation models should include poro-elasto-plastic rheology with thermal stresses and hardening-weakening effects, and include damage models when cycled loading-unloading is of interest (Figure 2). Another important factor for real world cases is seismic risk assessment, and in such cases a simulation tool should be able to adequately assess mechanistic seismic hazard, including expected maximum magnitude (Figure 3).

Numerical implementation of these models requires state of the art numerical schemes capable of dealing with complex geometries while maintaining high accuracy and numerical resolution.

Finite differences, finite volumes and mixed finite elements are well suited for fluid flow simulations in complex domains, while finite elements and mesh free methods have been applied for rock deformation simulations (Figure 4).

Solutions of these coupled models using advanced numerical schemes at high resolution is computationally expensive and requires very long computational times. Graphical Processor Units

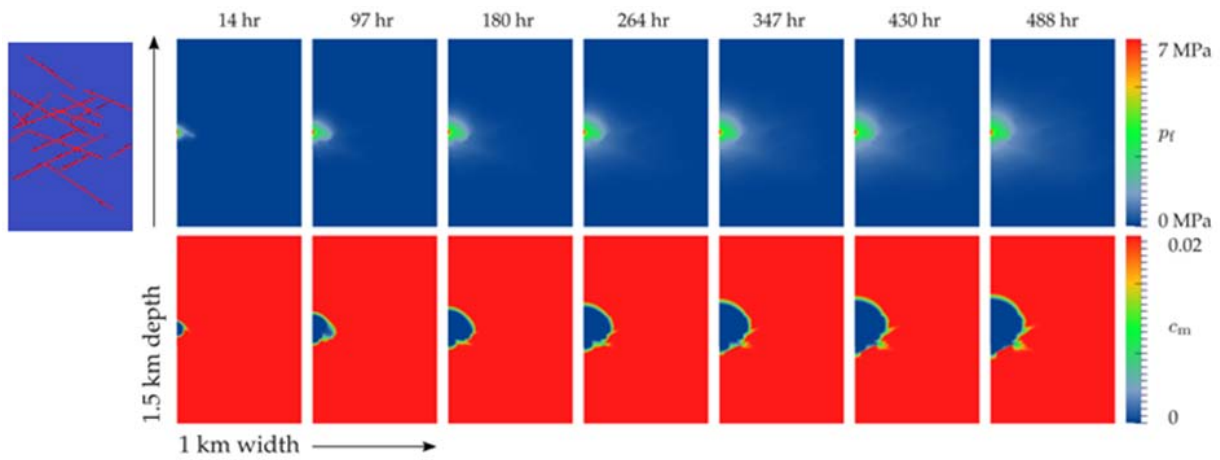


Fig. 1.: Results of a geothermal system simulation. Fresh cold water is injected in a hot fractured porous rock which is saturated with saline water. Figures on top show the pressure of the system while on bottom are the corresponding mass fraction diagrams

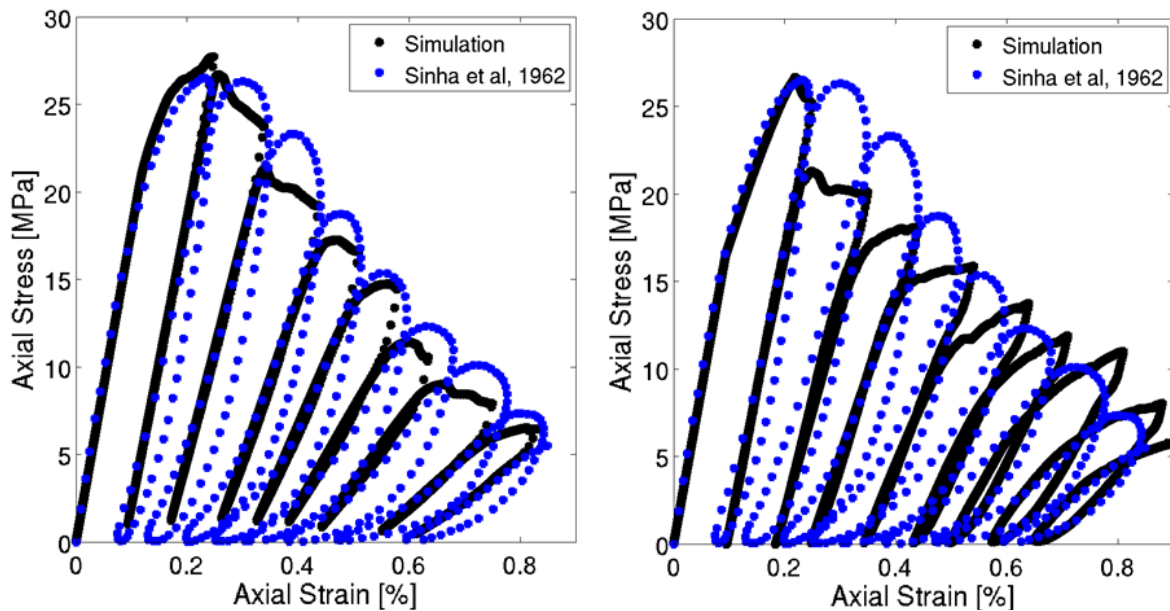
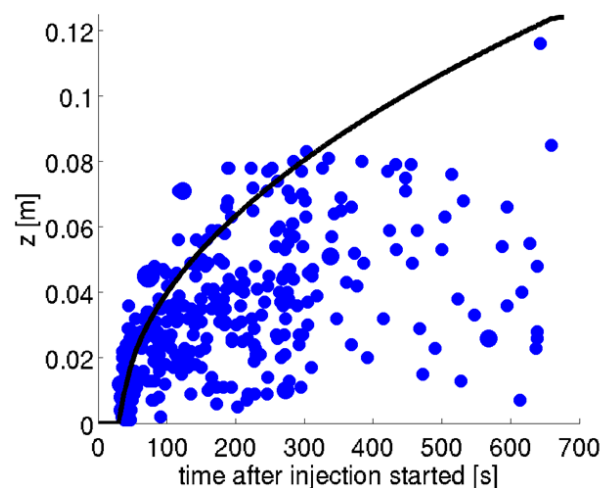


Fig. 2.: Comparison of two damage models with experimental data cycling compression test. A) Damage operator as a function of effective plastic strain. b) Double surface damage-yield functions model.



**Fig. 3.:** Propagation of acoustic emissions during fluid injection in a drained specimen. Results from poro-elasto-plastic model simulation. Black curve represent fluid front as solution of saturation equation. Blue dots are numerical acoustic emissions. Following experimental data from Stanchits et al. 2011.

(GPUs) resend a new programming paradigm that allows shorter computational times in comparison to CPU programming. However, for correct and efficient implementation of numerical algorithms in GPUs it is necessary to manage different memory protocols and specialized programming techniques, which adds additional complexity to the problem. In addition, usage of distributed GPU clusters for numerical simulations and even the implementation of well-known numerical algorithms, is a very new research area.

Under these circumstances of complex physical models and high numerical resolution, post processing may become a bottleneck. Fast analysis of the data requires fast and informative post processing techniques, and real time visualization techniques might allow rapid analysis of large data sets. In particular, for 3D simulations, visualization plays an important role. The question is how to present 3D information in the most informative way while maintaining computationally efficiency (Figure 5). Particularly for GPU systems, communication from GPUs to CPUs to apply rendering techniques slows down the entire computation, so new rendering algorithms appropriate for GPUs must be developed.

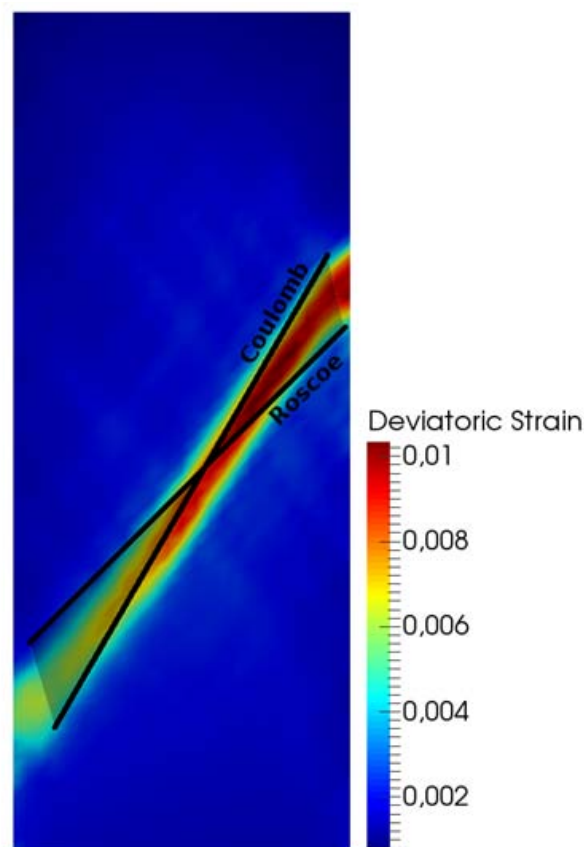


**Fig. 4.:** Shear bands for strain for uniaxial experiment simulation. Simulation of poro-elasto-plastic model using mesh free methods.

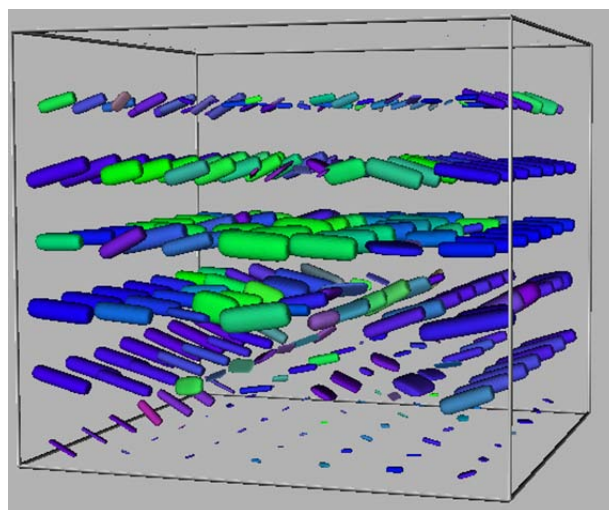


**Fig. 5.:** Visualization of 3D stress tensor using glyphs.

The description and representation of complex geometries, as they are encountered in real world cases, is a complicated task. Some tools rely on third party programs to create a suitable numerical representation of the geometry of the case under study. In other cases an over-simplification of the geometry is required. These procedures may result in limited applicability or usage of the simulation tool.

Tactile devices that allow a more intuitive and faster interaction with computational tools may increase the use of scientific simulation programs. Programming of a general multifunctional modeling tool for lithospheric fluid-rock processes is a very complex task. In this talk, we present different steps that we have taken toward this goal. This includes the development of new physical models, application to real cases and implementation of these models using advanced numerical schemes. We also describe some programming techniques for object oriented implementation in CPU, GPU and cluster of GPUs, pre-processing using tangible devices and visualization techniques for CPU and GPU based programs.



# THC modelling of an Enhanced Geothermal System

Sahar Hamidi, Thomas Heinze, Boris Galvan, Stephen Miller

*Geodynamics/Geophysics, University of Bonn*

**e-mail:** hamidi@geo.uni-bonn.de

**session:** Fluids and Deformation

Fluid-rock interactions play an essential role in many earth processes, from a likely influence on earthquake nucleation and aftershocks, to enhanced geothermal system, carbon capture and storage (CCS), and underground nuclear waste repositories. Coupled thermal-hydraulic-chemical models (THC) are important for investigating these processes. Our objective is to develop algorithms for coupling the fluid processes to the rock mechanics that control rock deformation and fracture. To that aim, we present a two-dimensional numerical simulation of a fully coupled non-isothermal non-reactive solute flow flexible for field as well as laboratory scales.

In THC models, two-way interactions between different processes (thermal, hydraulic and chemical) are present. Fluid flow influences the permeability of the rock especially if chemical reactions are taken into account. On one hand solute concentration influences fluid properties while, on the other hand, heat can affect further chemical reactions.

The flow process of the model includes a non-linear Darcian flow for either saturated or unsaturated scenarios. The governing equation for the saturated case is:

$$\frac{\partial}{\partial t} (\phi \rho) + \nabla (\rho \mathbf{v}) = Q \quad (1)$$

where  $\rho$  is the mass density of the fluid,  $\phi$  the rock porosity,  $Q$  the source/sink term and  $\mathbf{v}$  Darcy velocity:

$$\mathbf{v} = \frac{-\kappa}{\mu} (\nabla P - \rho \mathbf{g}) \quad (2)$$

where  $\kappa$  is the permeability,  $\mu$  the dynamic viscos-

ity of the fluid and  $\mathbf{g}$  the gravitational acceleration. For the variably saturated systems in laboratory scale, Richards' Approximation is used (Kolditz, 2002) and the relative permeabilities are derived from van Genuchten relations (van Genuchten, 1980). Permeability and porosity of rock are stress and pressure dependent (Rutqvist et al., 2002). Additionally, the gravitation effects can be switched on and off depending on the simulation case.

The non-reactive mass transport is described as (Ackerer et al., 1999) :

$$\phi \frac{\partial C_m}{\partial t} + \mathbf{v} \nabla C_m - \nabla (D_m \nabla C_m) = 0 \quad (3)$$

with  $C_m$  mass fraction and  $D_m$  molecular diffusion coefficient.

The thermal part of the simulation models heat transfer processes for either local thermal nonequilibrium or equilibrium cases. For the former one, conservation of energy for fluid and rock is expressed as (Shaik et al., 2011):

$$\phi c_{p,f} \rho_f \frac{\partial T_f}{\partial t} + \mathbf{v} \nabla T_f - \lambda_f \nabla^2 T_f + Q_T = 0 \quad (4)$$

$$(1 - \phi) c_{p,r} \rho_r \frac{\partial T_r}{\partial t} - \lambda_r \nabla^2 T_r - Q_T = 0 \quad (5)$$

$$Q_T = hA (T_f - T_r) \quad (6)$$

where  $T$  is temperature,  $c_p$  thermal capacity,  $\lambda$  thermal conductivity,  $Q_T$  heat transfer between rock and fluid,  $h$  heat transfer coefficient and  $A$  heat transfer area. Assuming local thermal equilibrium, we can rewrite the temperature equation (Kolditz, 2002):

$$c_p \rho \frac{\partial T}{\partial t} + c_{p,f} \rho_f \phi \mathbf{v} \nabla T - \lambda \nabla^2 T = 0 \quad (7)$$

$$c_p = \phi c_{p,f} \rho_f + (1 - \phi) c_{p,r} \rho_r \quad (8)$$

$$\lambda = \phi \lambda_f + (1 - \phi) \lambda_r \quad (9)$$

Estimating heat production from a naturally fractured geothermal systems remains a complex problem. Previous works are typically based on a local thermal equilibrium assumption and rarely consider the salinity. The dissolved salt in fluid affects the hydro- and thermodynamical behavior of the system by changing the hydraulic properties of the circulating fluid. For studying such a system, we consider a given fracture network saturated with saline water and inject high pressure fresh water into it. We compare the results of different assumptions (e.g. local thermal equilibrium an non-equilibrium) with field observations (Figure 2).

## References

- Ackerer et al. Modeling variable density flow and solute transport in porous medium: 1. Numerical model and verification. *Transport in Porous Media* 35.3 (1999): 345-373.
- Kolditz, Olaf. *Computational methods in environmental fluid mechanics*. Springer (2002)
- Rutqvist, J., et al. A modeling approach for analysis of coupled multiphase fluid flow, heat transfer, and deformation in fractured porous rock. *International Journal of Rock Mechanics and Mining Sciences* 39.4 (2002): 429-442.
- Shaik, Abdul Ravoof, et al. Numerical simulation of Fluid-Rock coupling heat transfer in naturally fractured geothermal system. *Applied Thermal Engineering* 31.10 (2011): 1600-1606.
- Stanchits, Sergei, et al. Fracturing of porous rock induced by fluid injection. *Tectonophysics* 503.1 (2011): 129-145
- Van Genuchten, M. Th. A closed-form equation for predicting the hydraulic conductivity of unsaturated soils. *Soil Science Society of America Journal* 44.5 (1980): 892-898.

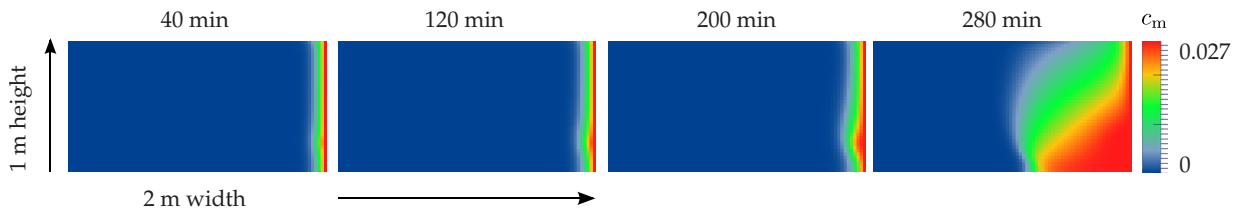


**Fig. 1.:** The Henry saltwater intrusion problem describes the steady state solution of a diffused saltwater front in an initially saturated fresh water confined aquifer. Results of the simulation for  $\kappa = 1 \times 10^{-12} \text{ m}^2$  and  $D_m = 1.886 \times 10^{-6} \text{ m}^2 \text{ s}^{-1}$ .

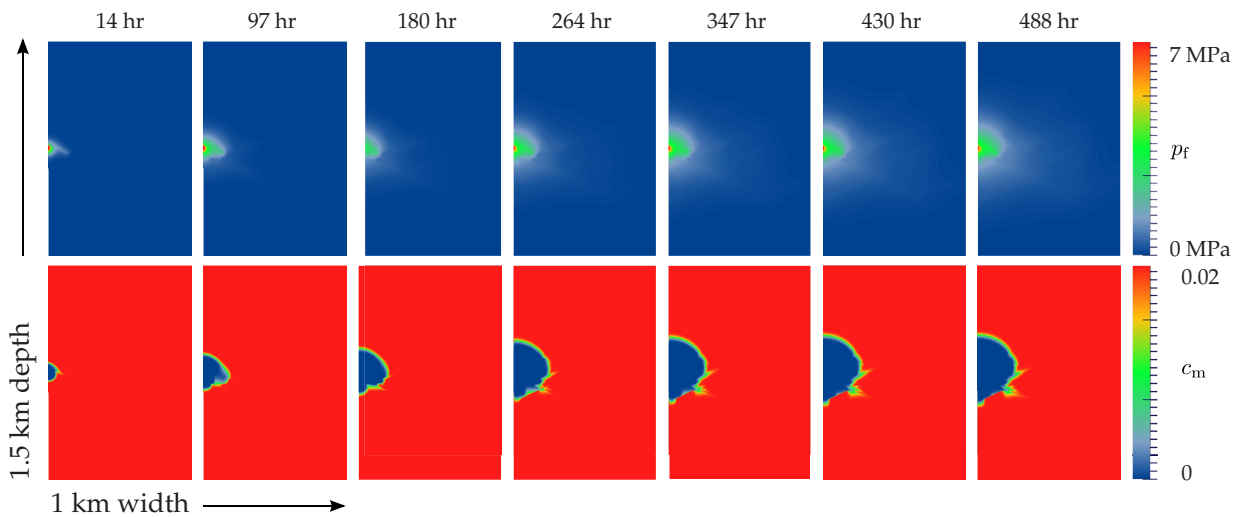


**Fig. 2.:** Results of a geothermal system simulation. Fresh cold water is injected in a hot fractured porous rock which is saturated with saline water. Figures on top show the pressure of the system while on bottom are the corresponding mass fraction diagrams.

# Numerical Modelling of earthquake swarms in the Vogtland / West-Bohemia

Thomas Heinze, Sahar Hamidi, Boris Galvan, Stephen Miller

*Geodynamics/Geophysics, Bonn University*

*e-mail: heinze@geo.uni-bonn.de*

*session: Fluids and Deformation*

## Introduction

An earthquake swarm is defined as a sequence without a single, dominant event (Yamashita, 1998). Field observations and numerical simulations suggest that fluid flow is an important component in the generation of earthquake swarms (Hainzl, 2004). In West Bohemia / Vogtland, earthquake swarms coincide with degassing of CO<sub>2</sub> originating from the mantle. Young Quaternary volcanism with a magmatic body associated with a local Moho updoming is the assumed source for the CO<sub>2</sub> that propagates through a pre-existing and re-stimulated fracture network (Weinlich et al., 1999). The fluids are suggested as a main trigger for earthquake activity in the region (e. g. Spicak & Horalek, 2001, Weise et al., 2001, Bräuer et al. 2003).

Earthquake swarms over the last decades concentrated in the Novy Kostel area (Czech Republic) within a region of several square kilometers. The earthquake swarms, with a maximum magnitude of 4.5, include several thousand micro-seismic events with hypocenters ranging between 6.5 km and 11 km, with some deeper around 13 km, and occur along a steeply dipping fault plane (Fischer & Horalek, 2003). Registered swarms occurred in 1985/1986, 1997, 2000, 2008 and 2011, during which previously ruptured areas were reactivated (Fischer et al., 2014).

Several numerical models have been applied to the West- Bohemian earthquake swarms, including a poro- elasto plastic finite element model to calculate stresses and strains (Kurz et al., 2003).

These studies demonstrated that the regional stress field is insufficient to cause earthquake swarms, but when combined with fluid migration they show reasonable rates of deformation capable of earthquake swarms. Statistical approaches can reproduce the seismic pattern of the 2000 swarm (Hainzl, 2004), where a brittle patch surrounded by an elastic half- space is loaded by fluid migration and stress changes. The spatio-temporal distribution of the seismic events is shown to be dominated by stress triggering, with fluid migration acting as the initiator. Linear diffusion models (Parotidis et al., 2005) focused on a single fluid source to determine overall diffusivity.

In this work we develop and apply a model to simulate the flow of supercritical CO<sub>2</sub> through a fracture network assuming non- linear diffusion with a stress and pressure dependent permeability and porosity (Rutqvist et al., 2002). We solve the diffusion-advection equations for the temperature of the rock and CO<sub>2</sub>, assuming local equilibrium. Stresses are calculated with a full poro-thermo-elasto- plastic rheological model taking hardening, softening and damage effects into account. Plastic deformation of rocks is modeled using the Griffith and Mohr-Coulomb criteria. Cohesion and internal friction angle are mobilized in terms of a cohesion weakening and frictional strengthening model (CWFS) (Hajiabdolmajid et al., 2002). The mobilized values for friction angle, cohesion and dilatancy angle are calculated as functions of the effective plastic stresses and a damage variable is calculated as a functions of plastic strain. Our theoretical model is implemented in

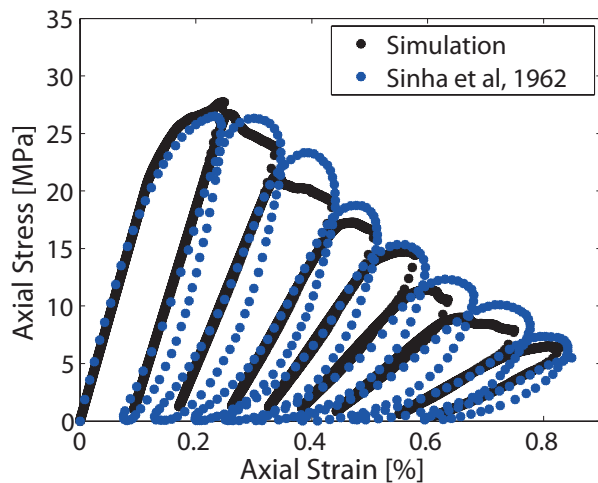


Fig. 1.: Comparison of experimental and simulated stress- strain response curve of an uniaxial compression cycling test of a concrete specimen. Experimental data taken from (Sinha et al., 1962).

a numerical scheme using finite differences on a staggered grid to simulate the dynamic behavior during loading and fluid injection. The numerical results of the model show very good agreement with laboratory results (figure 1). Coincidence was achieved for stress–strain relationships, volumetric and inelastic strain, fracture propagation and stress drop during fluid injection.

Estimating the seismic moment of a fracture generation or -propagation is of great interest in numerical simulations. Most published models are able to reproduce important features and behavior of the seismic events like the propagation of the seismic cloud from the borehole, the Kaiser- Effect and also give reasonable values for magnitudes and the overall distribution of the events. They are mainly tested at shale gas fields or geothermal sides.

We present an approach based on continuum mechanics to derive the seismic magnitude using the deviatoric strain as an indicator for rupture processes. A peak- detection algorithm is used to identify rapid changes that are then marked as seismic events. This method works very well on laboratory scale for dry and hydraulic fracturing (figure 2). In this work we apply the same mechanism to field scale to match the seismic characteristics of the earthquake swarm in the

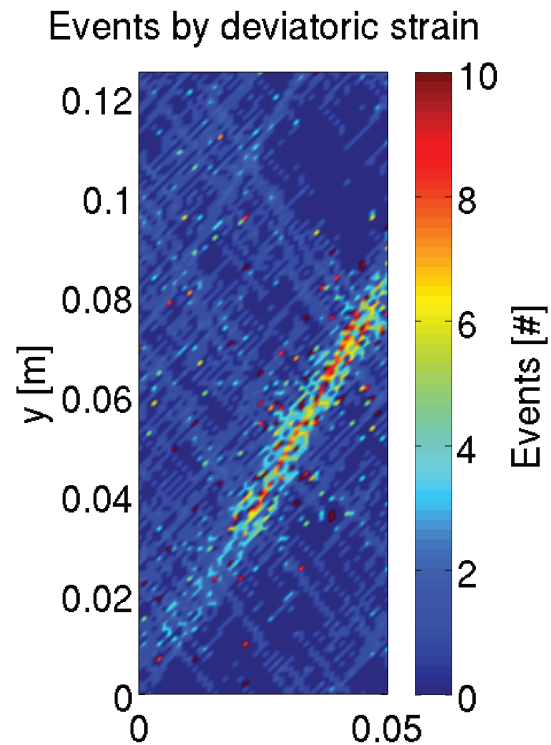


Fig. 2.: Numerical simulation of a confined compression experiment. Acoustic emissions are simulated using the deviatoric strain as a marker. Simulation results of acoustic emission fit to experimental observations (cf. Stanchits et al., 2011).

Vogtland / West Bohemia.

We numerically simulate the flow of hot, over-pressured CO<sub>2</sub> rising from below in a region from 5 km to 15 km depth mainly taking place in a preexisting fracture network (figure 3) which evolves during high pressure flow. We compare the results to field observations and the seismic measurements during the swarm activity, paying special attention to the seismic characteristics of the region.

## References

- Yamashita, T. (1998). Simulation of seismicity due to fluid migration in a fault zone. *Geophysical Journal International*, 132, p. 674-686.
- Hainzl, S. (2004). Seismicity patterns of earth-

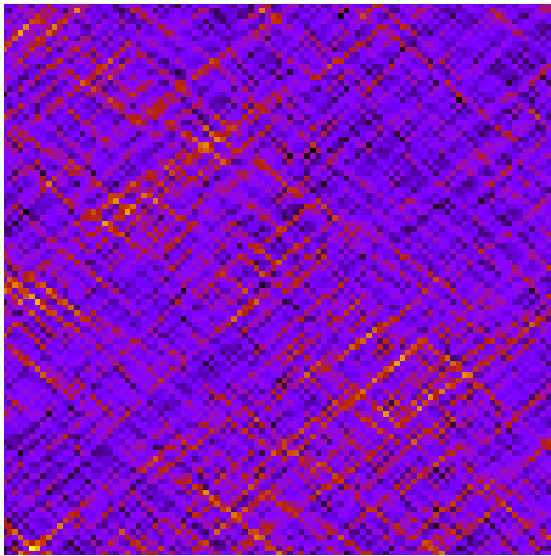


**Fig. 3.:** Deviatoric strain of a fracture network obtained from a numerical simulation of a compressive environment. Dimensions are 2 km x 2 km.

- quake swarms due to fluid intrusion and stress triggering. *Geophysical Journal International*, 159, p.1090-1096.
- Weinlich, F.H., Bräuer, K., Kämpf, H., Strauch, G., Tesar, J. Weise, S.M. (1999). An active subcontinental mantle volatile system in the western Eger rift, Central Europe: Gas flux, isotopic and compositional fingerprints. *Geochimica et Cosmochimica Acta*, 63(21), p. 3653-3671.
- Spicak, A., Horalek, J. (2001). Possible role of fluids in the process of earthquake swarm generation in the West Bohemia/Vogtland seismogenic region. *Tectonophysics*, 336, p.151-161.
- Weise, S.M., Bräuer, K., Kämpf, H., Strauch, G., Koch, U. (2001). Transport of mantle volatiles through the crust traced by seismically released fluids: a natural experiment in the earthquake swarm area Vogtland/NW Bohemia, Central Europe. *Tectonophysics*, 336, p.137-150.
- Bräuer, K., Kämpf, H., Strauch, G., Weise, S.M. (2003). Isotopic evidence ( $^3\text{He}/^4\text{He}$ ), of fluid-triggered intraplate seismicity. *Journal of Geophysical Research*. 108(82).
- Fischer, T., Horalek, J. (2003). Space-time distribution of earthquake swarms in the principal focal zone of the NW Bohemia/Vogtland seismogenic region: period 1985–2001. *Journal of Geodynamics*. 35, p. 125-144.
- Fischer, T., Horalek, J., Hrubcova, P., Vavrycuk, V., Bräuer, K., Kämpf, H. (2014). Intra-continental earthquake swarms in West-Bohemia and Vogtland: A review. *Tectonophysics*, 611, p.1-27.
- Kurz, J.H., Jahr, T., Jentzsch, G. (2003). Geodynamic modelling of the recent stress and strain field in the Vogtland swarm earthquake area using the finite element method. *Journal of Geodynamics*. 35, p. 247-258.
- Parotidis, M., Shapiro, S.A., Rothert, E. (2005). Evidence for triggering of the Vogtland swarms 2000 by pore pressure diffusion. *Journal of Geophysical Research*, 110.
- Rutqvist, J., Wu, Y.S., Tsang, C.F., Bodvarsson, G. (2002). A modeling approach for analysis of coupled multiphase fluid flow, heat transfer, and deformation in fractured porous rock. *International Journal of Rock Mechanics & Mining Sciences*, 39, p.429-442.
- Hajiabdolmajid, V., Kaiser, P.K., Martin, C.D. (2002). Modelling brittle failure of rock. *International Journal of Rock Mechanics & Mining Sciences*, 39, p.731-741.
- Sinha, B.P., Kurt, H. Gerstle, Tulin, L.G. (1964). Stress-Strain Relations for concrete under cyclic loading. *Journal of the American Concrete Institute*, 61(2), p.195-211.
- Stanchits, S., Mayr, S., Shapiro, S., Dresen, G. (2011). Fracturing of porous rock induced by fluid injection. *Tectonophysics*, 503, p.129-145.

# Modelling of fractured reservoirs: fluid-rock interactions within fault domains

Antoine Jacquey<sup>1</sup>, Mauro Cacace<sup>1,3</sup>, Guido Blöcher<sup>1</sup>, Magdalena Scheck-Wenderoth<sup>1,2</sup>

<sup>1</sup>*Helmoltz Centre Potsdam, GFZ German Research Center for Geosciences, Potsdam, Germany*

<sup>2</sup>*RWTH Aachen, Germany*

<sup>3</sup>*Potsdam University, Potsdam, Germany*

*e-mail:* [ajacquey@gfz-potsdam.de](mailto:ajacquey@gfz-potsdam.de)

*session:* *Fluids and Deformation*

The presence of a major fault can have significant impacts on the hydraulic and mechanical properties of the hosting rock. Different domains in terms of fluid and mechanical properties can be identified within a faulted region such as a low permeability fault core, a damage zone usually extending on both sides of the core where rocks are highly fractured and permeability increases and poorly fractured or intact rocks situated far away from the fault core [4, 7, 12], see figure 1. During geothermal operations, injection and production of fluid can induce significant pore pressure changes which impact the stress field thus affecting the reservoir rocks. In this context, the elastic and hydraulic properties of the porous rock can be altered by deformation of the pore and bulk volumes which in some cases may compromise the productivity of the geothermal system [3, 5]. Therefore special interest is given to porosity and permeability temporal evolutions as main properties controlling fluid transport processes within such systems.

The presence of fractures, their density, apertures and interconnectivity play a major role in affecting poroelastic processes within fault zones. While for a non fractured rock hydraulic properties will depend only on changes in pore volume as induced by elastic deformation of the pores, closure of fractures can induce important nonlinearities on the stress-strain relations [9]. Typical distributions are schematically shown in figure 1 for permeability (b) and Young's modulus (c).

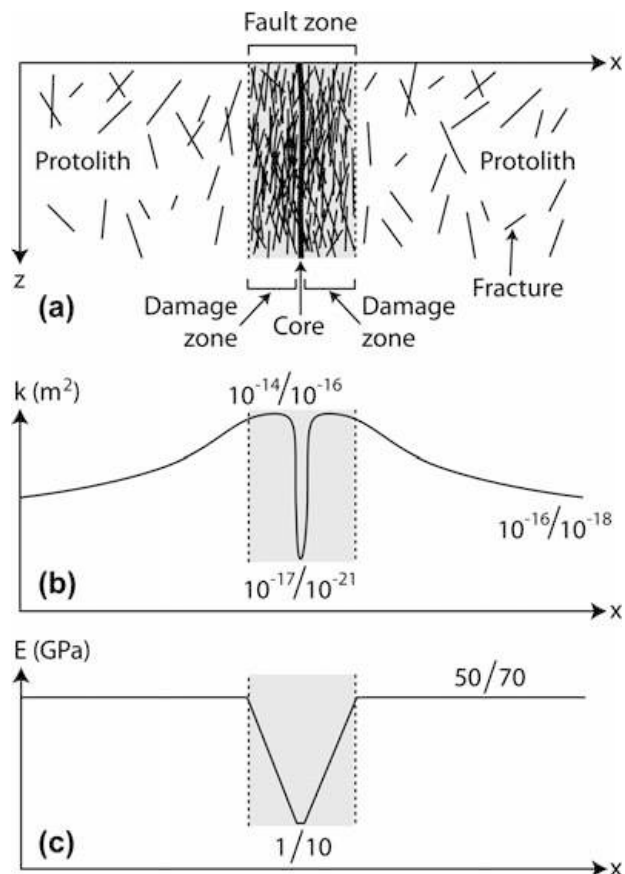


**Fig. 1.:** Fault zone configuration - example of the permeability and Young's modulus distributions [4]

Different behaviors in these two properties nicely illustrate how fractures may significantly impact processes occurring in these domains.

The aim of this project is to deepen current understanding of fundamental processes controlling fluid-rock interactions in fault zones. In a first step poroelastic formulations are derived which are based and validated on laboratory experiments on undamaged and damaged samples [2, 1, 8]. Porosity and permeability relations are the major focus of this project and their evolution is linked with the stress field or with pore pressure changes. An important interest will be given to the continuity of the formulations at the interface between two zones of the fault region. These formulations, implemented in a simulation software will be used in a future step to simulate a faulted geothermal system at the reservoir scale thus abling to analyze fluid-rock interactions within the fault and the impact of major fault zones on the system productivity.

Simulations are conducted using the open-source 3-D finite element method-based simulator OpenGeoSys [14, 16, 15, 10] which offers the possibility of solving coupled processes within a hybrid approach combining discrete fractures and continua models for fractured porous rocks. Porosity and permeability relations previously defined and validated have been implemented in the simulator.

The current results of the project will be presented, including porosity and permeability relations for undamaged samples. From [1], experimental data for porosity of two kinds of sandstone are presented. The availability of these data lead to first consider for this project these two sandstones: Flechtinger sandstone, a Lower Permian (Rotliegend) sedimentary rock from an outcrop near Flechtiner, Germany [11] and Bentheimer sandstone, a Lower Cretaceous sedimentary rock from an outcrop near Bentheim, Germany [6]. Unlike the Bentheimer sandstone which is very homogeneous (95% quartz, 3% kaolinite and 2% orthoclase), Flechtinger sandstone is composed of quartz (55–65%), rock fragments of volcanic origin (20–25%) and feldspars (15–20%). Different models [1, 13, 8] for sandstones have

been investigated and compared to the laboratory measurements. From [13], porosity changes depend on the mean effective stress:

$$\phi = (\phi_0 - \phi_r) e^{A\sigma'_M} + \phi_r \quad (1)$$

Where  $\phi_0$  and  $\phi_r$  are the initial and residual porosity (at high stresses),  $\sigma'_M$  the mean effective stress and  $A$  a coefficient. And from [1], porosity changes depend on drained experiment quantities such as the drained volumetric strain (equation (2)) or the drained bulk compressibility (equation (3)):

$$\phi = \frac{V_\phi^0 - e_V V_b^0 + e_V^u (V_b^0 - V_\phi^0)}{V_b^0 - e_V V_b^0} \quad (2)$$

$$d\phi = -((1 - \phi_0) C - C_s^u) dp_e \quad (3)$$

Where  $V_\phi^0$  and  $V_b^0$  are initial pore and bulk volumes,  $e_V$  and  $e_V^u$  the volumetric strains under drained and unjacketed conditions.  $C$  is the drained bulk compressibility,  $C_s^u$  the unjacketed solid compressibility and  $p_e$  the Terzaghi effective pressure.

The validity of new poroperm relations is tested by simulating isothermal hydrostatic tests with increasing pore pressure on 3-D cylindrical rock samples under the same conditions as the laboratory experiments (see figure 2). In such configuration, the confining pressure is equal to the pore pressure. Experimental results from a drained hydrostatic test are used for some of the models in order to obtain poroperm relations fitting laboratory measurements [9]. An acting pressure from 0.1 MPa up to 70 MPa is considered with an increasing rate of 10 MPa h<sup>-1</sup>. In these conditions the porosity decreases with increasing acting pressure due to changes in pore and bulk volumes.

Figure 3 shows the porosity evolution depending on the acting pressure for an undamaged sample of Flechtinger sandstone (sub-figure 3 a) and Bentheimer sandstone (sub-figure 3 b). For an acting pressure of 70 MPa, a decrease of 8,1% and 1,4% for the Flechtinger sandstone and for the Bentheimer sandstone are respectively observed. Two different domains are identified: under a certain acting pressure (20 MPa



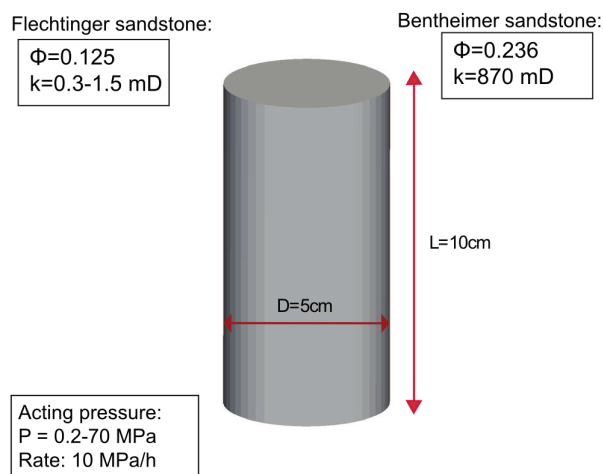


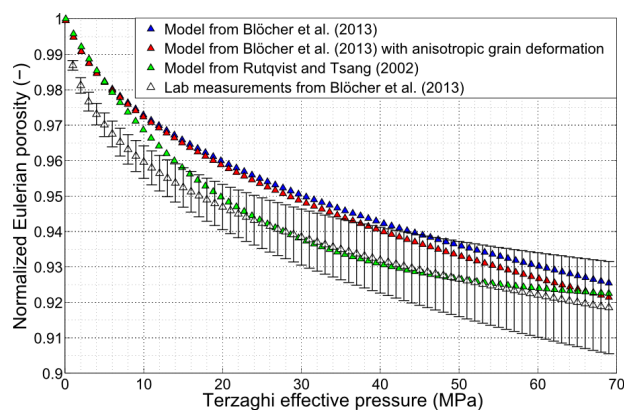
**Fig. 2.:** Simulation setup of the hydrostatic test and initial properties of the two sandstones

for Flechtinger sandstone and 10 MPa for Bentheimer sandstone) the porosity decreases non-linearly and linearly above this acting pressure. These two domains can be identified in the porosity computed with models from [1] but the model from [13] gives a better precision for the porosity in the considered acting pressure range. These results show that the porosity of the Flechtinger sandstone is more sensitive to a change of pore pressure than the porosity of the Bentheimer sandstone.

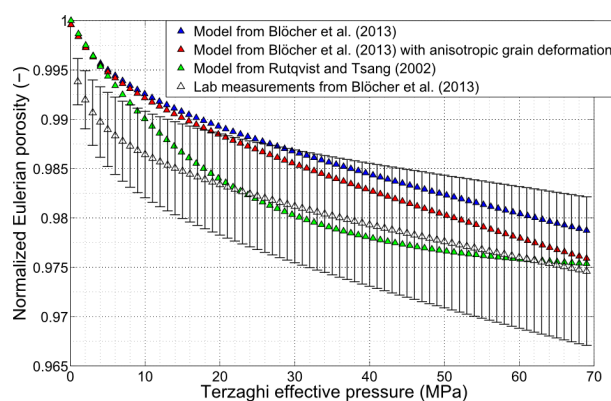
Permeability changes are linked to porosity changes and pore shape changes using the Kozeny-Carman permeability derived from the Hagen-Poiseuille equation. Following this approach, permeability changes can be expressed as a function of porosity changes and a Kozeny-Carman coefficient [9]:

$$k = A \frac{\phi^3}{(1 - \phi)^2} \quad (4)$$

Where  $A$  is a parameter which depends on the geometry of the pore and  $\phi$  is the porosity. In [2], this poroperm relation has been evaluated for the Flechtinger sandstone and validated by comparison with experimental measurements of permeability. Figure 4 shows the computed permeabilities computed with equation (4). With this model, the permeability decrease shows the same evolution trend as for the porosity. A de-



**(a)** Flechtinger sandstone



**(b)** Bentheimer sandstone

**Fig. 3.:** Normalized porosity evolution for the two mentioned sandstones

crease of 27% and 8% for the Flechtinger and Bentheimer sandstones permeability respectively are observed for an acting pressure of 70 MPa. Such decrease can have significant impacts on fluid flow and accordingly also on a geothermal system productivity.

Different models have been tested for porosity and permeability changes under increasing pore pressure after being implemented in the finite element method-based simulator OpenGeoSys. Models for porosity which depend on measurements made in laboratory under drained conditions show a good trend but are strongly dependent on the available experimental data. In future work, changes for mechanical properties such as the bulk compressibility will be investigated for undamaged samples to generalize these porosity relations for different kind of sandstones. Then

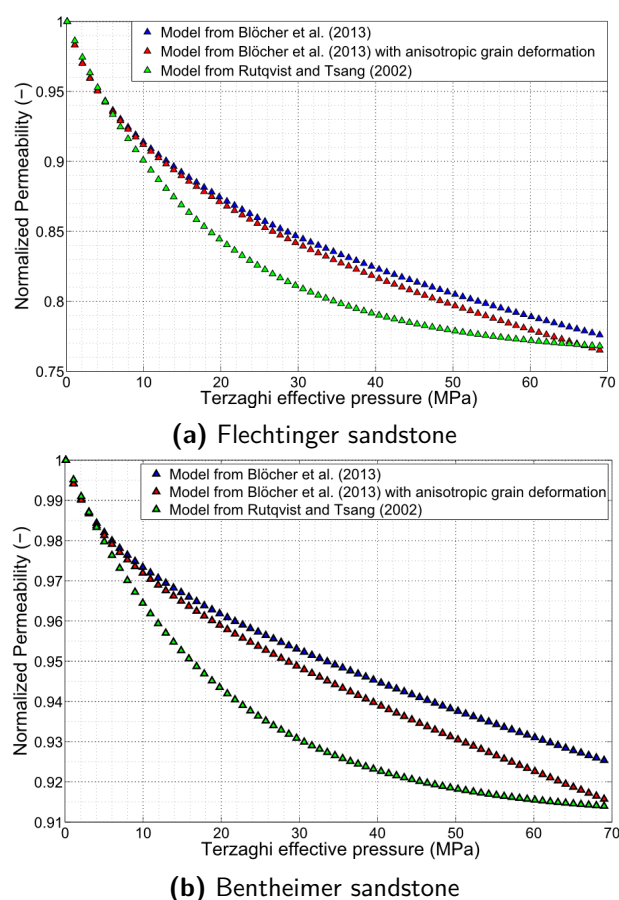


**Fig. 4.:** Normalized permeability evolution for the two mentioned sandstones

in next steps, the study of damaged sandstones will be performed in parallel with laboratory experiments with different fractures densities to complete the fault zone model.

## References

- [1] Guido Blöcher, Thomas Reinsch, Alireza Hassanzadegan, Harald Milsch, and Günter Zimmermann. Direct and indirect laboratory measurements of poroelastic properties of two consolidated sandstones. *International Journal of Rock Mechanics and Mining Sciences*, 67:191–201, April 2013.
- [2] Guido Blöcher, Günter Zimmermann, and Harald Milsch. Impact of Poroelastic Response of Sandstones on Geothermal Power Production. *Pure and Applied Geophysics*, 166(5-7):1107–1123, May 2009.
- [3] Mauro Cacace, Guido Blöcher, Norihiro Watanabe, Inga Moeck, Nele Börsing, Magdalena Scheck-Wenderoth, Olaf Kolditz, and Ernst Huenges. Modelling of fractured carbonate reservoirs: outline of a novel technique via a case study from the Molasse Basin, southern Bavaria, Germany. *Environmental Earth Sciences*, 70(8):3585–3602, March 2013.
- [4] Frédéric Cappa. Modelling fluid transfer and slip in a fault zone when integrating heterogeneous hydromechanical characteristics in its internal structure. *Geophysical Journal International*, 178(3):1357–1362, September 2009.
- [5] Y. Cherubini, Mauro Cacace, Magdalena Scheck-Wenderoth, and V. Noack. Influence of major fault zones on 3-D coupled fluid and heat transport for the Brandenburg region (NE German Basin). *Geothermal Energy Science*, 2(1):1–20, April 2014.
- [6] Jeremie Dautriat, Nicolas Gland, Jean Guelard, Alexandre Dimanov, and Jean L. Raphanel. Axial and Radial Permeability Evolutions of Compressed Sandstones: End Effects and Shear-band Induced Permeability Anisotropy. *Pure and Applied Geophysics*, 166(5-7):1037–1061, May 2009.
- [7] D.R. Faulkner, C.a.L. Jackson, R.J. Lunn, R.W. Schlische, Z.K. Shipton, C.a.J. Wibberley, and M.O. Withjack. A review of recent developments concerning the structure, mechanics and fluid flow properties of fault zones. *Journal of Structural Geology*, 32(11):1557–1575, November 2010.
- [8] Alireza Hassanzadegan, Guido Blöcher, Harald Milsch, Luca Urpi, and Günter Zimmermann. The Effects of Temperature and Pressure on the Porosity Evolution of Flechtinger Sandstone. *Rock Mechanics and Rock Engineering*, 47(2):421–434, April 2013.
- [9] Alireza Hassanzadegan and Günter Zimmermann. A Poroelastic Description of Permeabil-

- ity Evolution. *Pure and Applied Geophysics*, October 2013.
- [10] O. Kolditz, S. Bauer, L. Bilke, N. Böttcher, J. O. Delfs, T. Fischer, U. J. Görke, T. Kalbacher, G. Kosakowski, C. I. McDermott, C. H. Park, F. Radu, K. Rink, H. Shao, H. B. Shao, F. Sun, Y. Y. Sun, a. K. Singh, J. Taron, M. Walther, W. Wang, N. Watanabe, Y. Wu, M. Xie, W. Xu, and B. Zehner. OpenGeoSys: an open-source initiative for numerical simulation of thermo-hydro-mechanical/chemical (THM/C) processes in porous media. *Environmental Earth Sciences*, 67(2):589–599, February 2012.
- [11] Harald Milsch, Guido Blöcher, and Silvio Engelmann. The relationship between hydraulic and electrical transport properties in sandstones: An experimental evaluation of several scaling models. *Earth and Planetary Science Letters*, 275(3-4):355–363, November 2008.
- [12] T.M. Mitchell and D.R. Faulkner. The nature and origin of off-fault damage surrounding strike-slip fault zones with a wide range of displacements: A field study from the Atacama fault system, northern Chile. *Journal of Structural Geology*, 31(8):802–816, August 2009.
- [13] J. Rutqvist, Y.-S. Wu, C.-F. Tsang, and G. Bodvarsson. A modeling approach for analysis of coupled multiphase fluid flow, heat transfer, and deformation in fractured porous rock. *International Journal of Rock Mechanics and Mining Sciences*, 39(4):429–442, June 2002.
- [14] Wenqing Wang and Olaf Kolditz. Object-oriented finite element analysis of thermo-hydro-mechanical ( THM ) problems in porous media. *International Journal for Numerical Methods in Engineering*, 69(May 2006):162–201, 2007.
- [15] Nori Watanabe, W Wang, J Taron, U. J. Görke, and O Kolditz. Lower-dimensional interface elements with local enrichment : application to coupled hydro-mechanical problems in discretely fractured porous media. *International Journal for Numerical Methods in Engineering*, pages 1010–1034, 2012.
- [16] Norihiro Watanabe, Wenqing Wang, Christopher I. McDermott, Takeo Taniguchi, and Olaf Kolditz. Uncertainty analysis of thermo-hydro-mechanical coupled processes in heterogeneous porous media. *Computational Mechanics*, 45(4):263–280, November 2009.

# Heat transport mechanisms at different scales – a 3D modelling workflow

Magdalena Scheck-Wenderoth<sup>1,2</sup>, Mauro Cacace<sup>1,3</sup>, Judith Sippel<sup>1</sup>, Yuriy Petrovich Maystrenko<sup>1,4</sup>, Yvonne Cherubini<sup>1,3</sup>, Vera Noack<sup>1,3,5</sup>, Björn Onno Kaiser<sup>1,3,6</sup>, Björn Lewerenz<sup>1</sup>

<sup>1</sup>*Helmholtz Centre Potsdam GFZ German Research Centre for Geosciences, Telegrafenberg, D-14473 Potsdam, Germany*

<sup>2</sup>*RWTH Aachen, Germany*

<sup>3</sup>*Potsdam University, Potsdam, Germany*

<sup>4</sup>*Geological Survey of Norway (NGU), Trondheim, Norway*

<sup>5</sup>*Bundesanstalt für Geowissenschaften und Rohstoffe, Dienstbereich Berlin, Germany*

<sup>6</sup>*DHI-WASY GmbH, Berlin, Germany*

**e-mail:** *sippel@gfz-potsdam.de*

**session:** *Fluids and Deformation*

Temperature plays a crucial role for many processes affecting the lithosphere, from fluid-rock interactions on the micro scale to the rheology-dependent deformation of an entire lithospheric plate. The thermal field of the lithosphere is controlled by heat transport mechanisms – namely conduction, advection, and convection – with diverse relative importance at different scales. We compare differently detailed 3D structural models from the Central European Basin System (CEBS) to assess the sensitivity of temperatures to (1) the heat transport mechanisms considered, (2) the configuration of the lithosphere in terms of 3D distribution of thermal and hydraulic properties and (3) fault-controlled groundwater flow. Based on the analysis of differently scaled models, we propose a strategy for modelling the geothermal field of sedimentary basins from the lithospheric to the local (reservoir) scale (Scheck-Wenderoth et al., 2014). This workflow has a hierarchical structure and shows how the results of larger scale simulations can be used as input and boundary conditions for smaller and more detailed models. The general applicability of this workflow and the resulting 3D temperature distributions make

it of interest for a broad range of geoscientific studies including thermo-mechanical modelling of lithospheric deformation or geothermal utilisation.

3D thermal models of the entire CEBS (e.g. Scheck-Wenderoth & Maystrenko, 2013; Fig. 1, 2) have shown that conduction is the dominant heat transport mechanism on the lithospheric scale. The thermal field is thus strongly controlled by the distribution of thermal conductivities caused by compositional and thickness variations of the highly conductive lithospheric mantle and crystalline crust as well as the insulating sedimentary cover. Among the sediments, rock salt plays an exceptional role because of its strongly varying thicknesses in the region and its very high thermal conductivity, which together produce strong (even though short-wavelength) thermal anomalies. Variable thicknesses of the upper crystalline crust induce thermal anomalies of larger wavelengths related to the large amount of radiogenic heat produced by these felsic rocks. Finally, the depth distribution of the thermal lithosphere-asthenosphere boundary (LAB) controls the basin-wide temperature distribution as

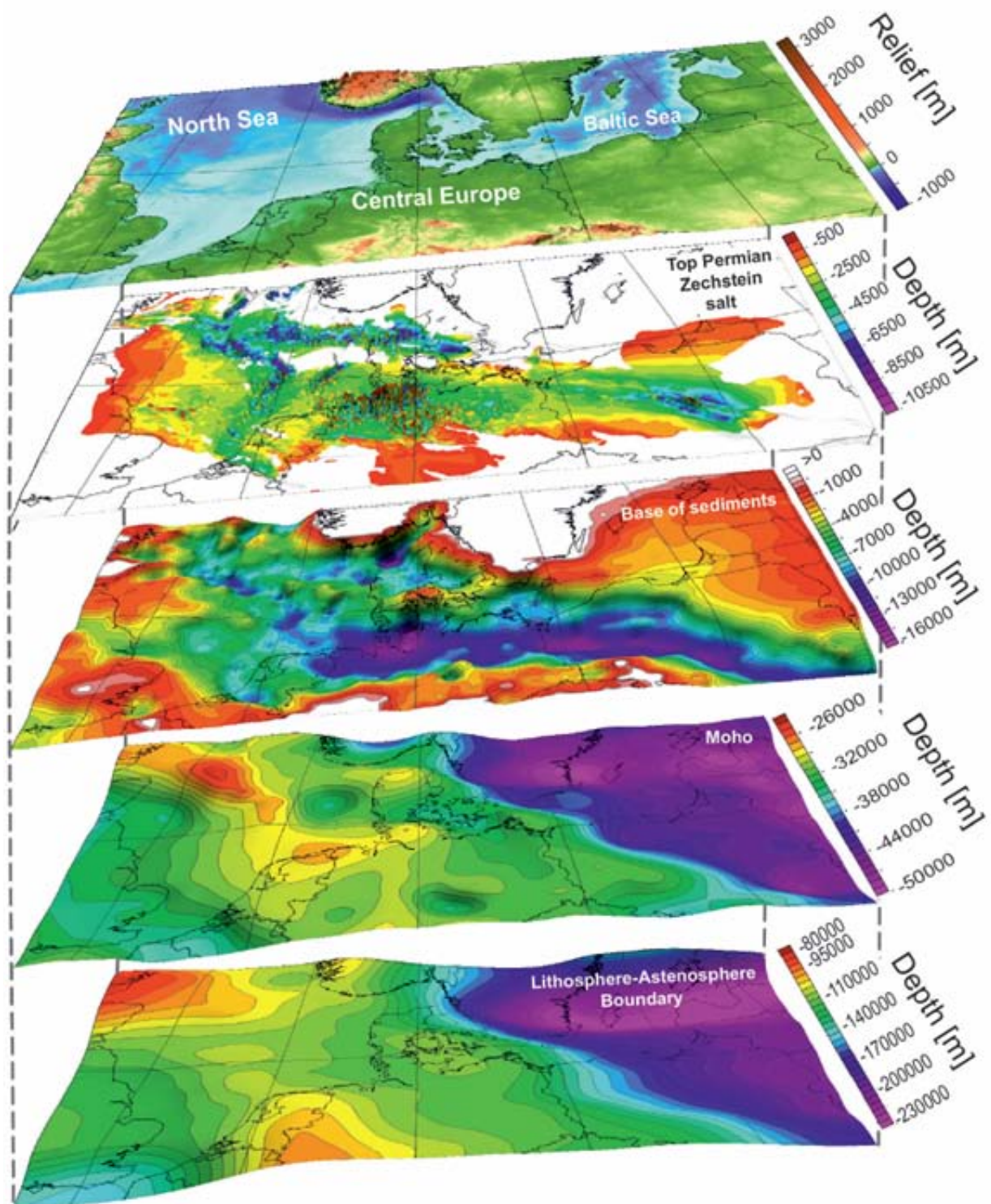


**Fig. 1.:** 3D structural model of the CEBS used for purely conductive thermal simulations (Scheck-Wenderoth & Maystrenko, 2013). The selected surfaces are relevant for the thermal field. The lithosphere-scale model covers an area of about 1000x1800 km with a horizontal resolution of ~4 km. It resolves eight sedimentary units (including a layer of mobilised Upper Permian Zechstein salt), two layers of the crystalline crust and the lithospheric mantle (after Maystrenko & Scheck-Wenderoth, 2013).

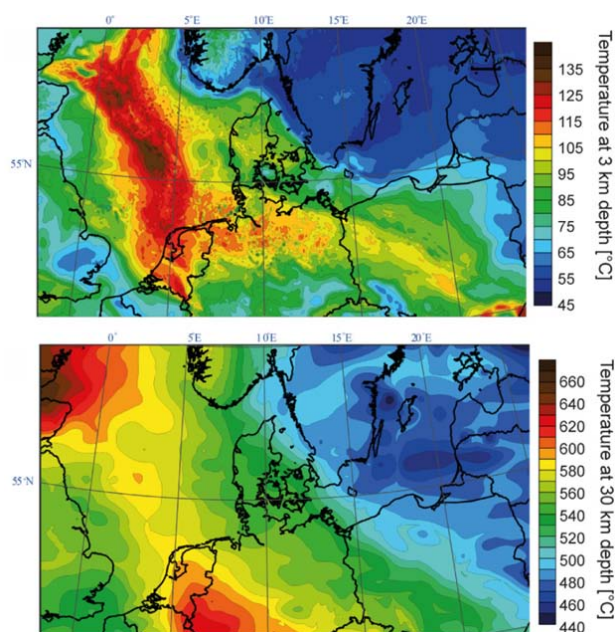


**Fig. 2.:** Results of the 3D thermal model of the CEBS with modelled temperature at 3 km and 30 km depth (below sea level; Scheck-Wenderoth & Maystrenko, 2013).

it represents the depth of commencing partial melting of the mantle and thus an isotherm (of  $\sim 1300^\circ\text{C}$ ). Knowing the depth of this isotherm thus provides a suitable lower boundary condition for thermal models of entire sedimentary basins.

The same factors (thermal conductivity, radiogenic heat production, and depth of the LAB) decide upon the distribution of temperatures on the regional scale, such as over the subsurface of the federal state of Brandenburg (e. g. Noack et al., 2012). For this reason, it is essential to consider information on the configuration of the deep crust and upper mantle also on the regional scale. However, local deviations of modelled temperatures from measured (borehole) temperatures also provide indications for moving fluids. Modelling the coupled transport of heat and fluid is numerically far more expensive and requires higher resolution of the subsurface geology and hydrogeology. Therefore, only models of a limited size can be studied with such simulations. Accordingly, the influence of fluid flow on the regional thermal field was successfully assessed for the area of Brandenburg down to a depth of

6 km (below sea level; Noack et al., 2013), thereby using well-constrained lower boundary conditions derived from lithosphere-scale thermal models of the CEBS.

On the local scale, groundwater flow and the corresponding temperature and pressure distributions might be influenced by the existence of faults and the related variations in hydraulic properties (Cherubini et al., 2014). Permeable faults may focus fluid flow and cause local convective instabilities along the fault area. Furthermore, 3D models show that free (density-driven) convection can occur locally, namely where the permeability and the thickness of geological layers are large enough and the hydraulic gradients low (e. g. Kaiser et al., 2011). To numerically reproduce such local processes related to coupled heat and groundwater transport along faults or the development of stable convective cells, even higher-resolved 3D models are required providing a high degree of detail on the distribution of hydraulic properties. Again, results from larger scale models can be exploited to extract suitable thermal and hydraulic boundary conditions for local high-resolution models.

## References

- Cherubini, Y., Cacace, M., Scheck-Wenderoth, M., Noack, V. (2014): Influence of major fault zones on 3-D coupled fluid and heat transport for the Brandenburg region (NE German Basin). *Geoth. Energ. Sci.*, 2, 1–20, 2014; doi:10.5194/gtes-2-1-2014.
- Kaiser, B. O., Cacace, M., Scheck-Wenderoth, M., Lewerenz, B. (2011): Characterization of main heat transport processes in the Northeast German Basin: Constraints from 3D numerical models. *Geochemistry, Geophysics, Geosystems* 12 (7), 1-17; doi:10.1029/2011GC003535.
- Maystrenko, Y. P., Scheck-Wenderoth, M. (2013): 3D lithosphere-scale density model of the Central European Basin System and adjacent areas. *Tectonophysics* 601, 53-77.

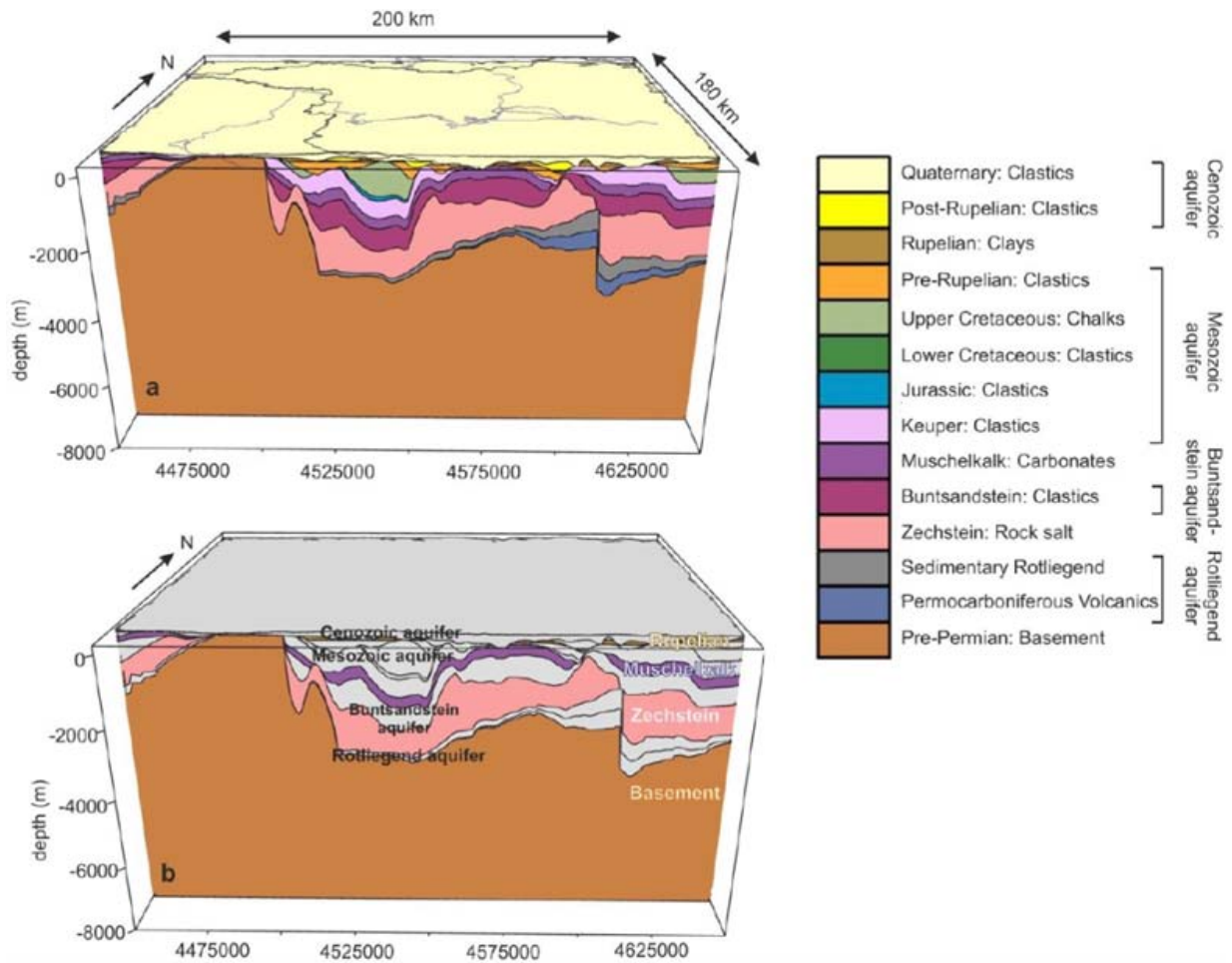
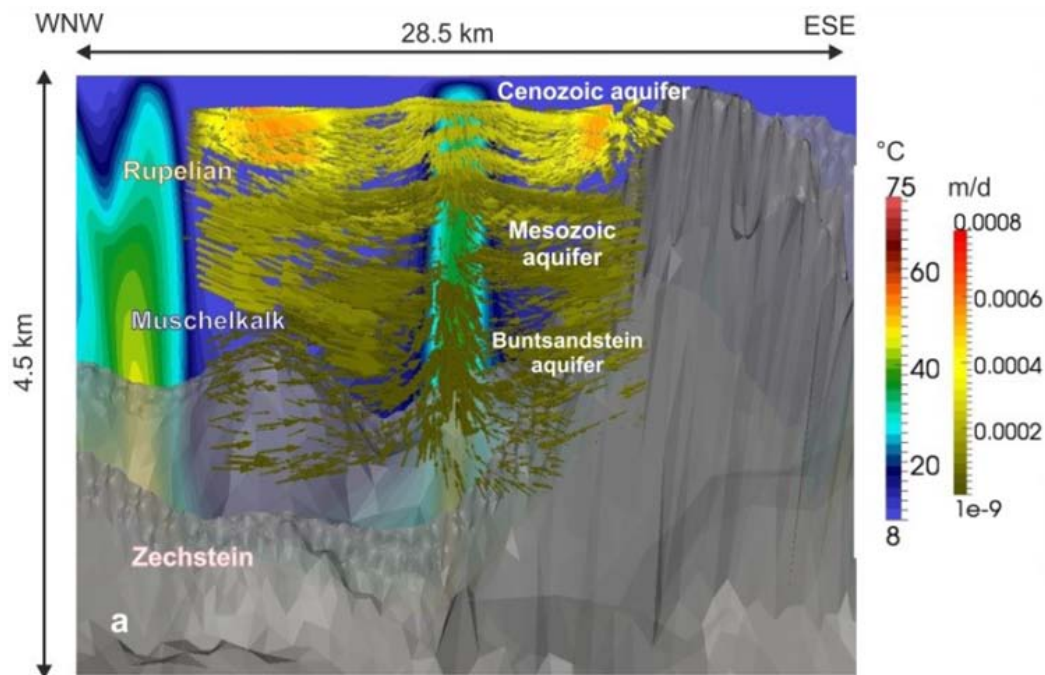


Fig. 3.: 3D geological model of Brandenburg (Noack et al., 2013) used for 3D coupled fluid and heat simulations (e. g. Cherubini et al., 2014); a) stratigraphic layers; b) aquitards (white) and aquifers (black).



**Fig. 4.:** 3D flow field around a permeable fault zone (Cherubini et al., 2014). Grey-shaded is the impervious Permian Zechstein salt layer. The Gardelegen fault zone is presented by its temperature distribution in the background. Groundwater flow is directed from the surrounding aquifers towards the fault zone (velocity vectors).

Noack, V., Scheck-Wenderoth, M., Cacace, M. (2012): Sensitivity of 3D thermal models to the choice of boundary conditions and thermal properties: a case study for the area of Brandenburg (NE German Basin). *Environ. Earth. Sci.* (2012) 67:1695–1711; doi: 10.1007/s12665-012-1614-2.

Noack, V., Scheck-Wenderoth, M., Cacace, M., Schneider, M. (2013): Influence of fluid flow on the regional thermal field: results from 3D numerical modelling for the area of Brandenburg (North German Basin). *Environ. Earth. Sci.* (2013) 70: 3523-3544, doi: 10.1007/s12665-013-2438-4.

Scheck-Wenderoth, M., Maystrenko, Y. P. (2013): Deep control on shallow heat in sedimentary basins. *Energy Procedia* 40, 266-275.

Scheck-Wenderoth, M., Cacace, M., Maystrenko, Y. P., Cherubini, Y., Noack, V., Kaiser, B. O., Sippel, J., Lewerenz, B. (2014): Models

of heat transport in the Central European Basin System: Effective mechanisms at different scales. *Marine and Petroleum Geology*, doi: 10.1016/j.marpetgeo.2014.03.009.



# Digital rock physics: Insight into fluid flow and elastic deformation of porous media

Takeshi Tsuji

*International Institute for Carbon-Neutral Energy Research, Kyushu University*

*e-mail: tsuji@i2cner.kyushu-u.ac.jp*

*session: Fluids and Deformation*

## Introduction

Digital rock physics combines modern microscopic imaging with numerical simulation for analysis of the physical and hydrological properties (e. g., Saenger et al., 2011). Recent technology developments of X-ray microcomputed tomography (micro-CT) as well as computational capacity for numerical simulation enable us to apply digital rock physics to realistic rock samples. Using digital pore models (Fig. 1), we study porous flow, fluid-solid interaction, interfacial phenomena, elastic and inelastic deformation, and mineral precipitation within real pore space. Since it allows us to estimate hydrological and elastic properties under several subsurface conditions (e. g., pressure), we can conduct virtual laboratory experiments in various reservoir conditions (e. g., Saenger et al., 2010; Tsuji et al., 2012; Jiang et al., 2014).

Here we mainly show the application of digital rock physics for Carbon dioxide Capture and Storage (CCS). In CCS projects, CO<sub>2</sub> injected into the subsurface reservoir can be trapped according to several mechanisms, including structural and stratigraphic trapping, capillary trapping, dissolution, and chemical reaction (or mineral precipitation). The behavior of CO<sub>2</sub> inside pore space can be characterized as two-phase flow in a porous media system, which is usually influenced by interfacial tension, pore structure, pressure, wettability, and etc. Therefore, we believe that digital rock physics significantly contributes to reveal multi-phenomena in porous medium oc-

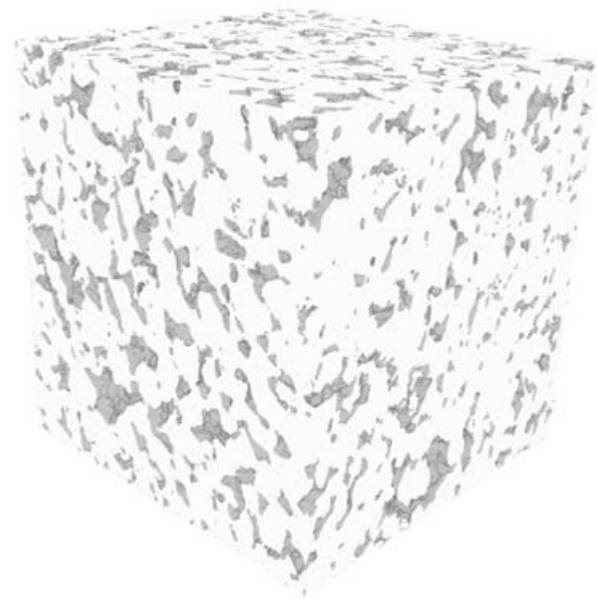


**Fig. 1.:** Three-dimensional pore geometry of Berea sandstone reconstructed from scanned micro tomographic image. Gray indicates the pore space.

curred in the CCS project.

To characterize properties of CO<sub>2</sub> injection reservoirs, we can apply digital rock physics to geophysical properties (e. g., seismic velocity). We usually use rock physics models (analytical models; Tsuji and Iturrino, 2008) or empirical relations (Tsuji et al., 2011) in order to estimate physical properties from seismic velocity. Using rock physics models, for example, we predict pore pressure distribution from high-resolution seismic velocity derived from waveform tomography (Tsuji et al., 2014). However, the analytical models (e. g., differential effective medium theory) can

be applied only for the limited or simplified pore geometry (e. g., crack). The digital rock physics can construct the relationship between elastic properties and subsurface properties by considering realistic pore geometry and various reservoir conditions. Here we also show our recent studies of digital rock physics to construct the relationship between elastic properties and subsurface properties under several conditions (Tsuji et al., 2012).

To predict long-term CO<sub>2</sub> behavior within the reservoir in CCS projects, we use reservoir simulation. A key parameter in the reservoir simulation is "relative permeability". Although the hydrological properties are significantly influenced by mineral precipitation due to CO<sub>2</sub> injection (e. g., change of pore space) and dissolution, it is difficult to estimate time evolution of these properties. The elastic properties (e. g., P-wave velocity) derived from time-lapse seismic survey are also influenced by mineral precipitation. Using digital rock approach, we can simulate mineral precipitation and estimate time-evolution of (1) hydrological properties (e. g., relative permeability) for reservoir simulation and (2) elastic properties for geophysical monitoring. Recently we have developed numerical calculation methods to model carbonate precipitation during long-term CO<sub>2</sub> storage (Jiang and Tsuji, in revision).

## Digital rock model

The digital rock model used in this study was extracted from images of a cylindrical core of Berea sandstone obtained by multi-slice micro-CT scanner (Fig. 1). Berea sandstone is well-sorted sandstone with relatively large size of grain. The resolution of the scanned images is 3.2 μm. Total data sets are composed of 396 slices with interval of 5 μm. In the image data, each pixel corresponds to CT value, which is proportional to the density of the material. To identify and label the pore and grain phases within the images, the segmentation process is carried out by using a single grayscale threshold method to match typical porosity of Berea sandstone (~21%). Con-

sequently, these segmented 2D pixel images are linearly interpolated to generate voxel-based 3D volume with 3.2 μm (Fig. 1).

## Two-phase LBM modeling

The fluid velocity field within the 3D pore spaces is calculated using the two-phase lattice Boltzmann method (LBM). In this study, we show the results using the color gradient model (Tölke et al., 2006) to treat the multi-phase problem. No-slip boundary conditions are imposed at all solid nodes including the precipitated minerals via a half-way bounce-back scheme. To increase the computation efficiency, we applied the graphics processor unit (GPU) parallel computing technique (e. g., Jiang et al., 2014). The advantages of GPU computing, including large memory bandwidth and low cost, make it suitable for conducting large-scale computation on a small-scale GPU-based cluster (Tölke and Krafczyk, 2008). Using this technique, we can conduct two-phase LBM simulation for the largest grid size in the world (~1000<sup>3</sup>; Fig. 2). The two-phase LBM simulation was often applied to the pore-scale model in order to characterize fluid flow within one pore throat with micrometer scale. Due to the GPU utilization, however, size of the digital rock is approaching to laboratory-scale (~centimeter scale). Therefore, the GPU computation could bridge a gap between pore-scale phenomena and laboratory-scale phenomena.

We estimate hydrological properties under several reservoir conditions (e. g., interfacial tension) from CO<sub>2</sub> behavior within pore space (Fig. 3). The relative permeability decreases with increasing IFT because of growing capillary trapping intensity (Fig. 3). In extremely low IFT conditions, the capillary trapping phenomenon disappears, and the curvatures of the relative permeability curves diminish (Jiang et al., 2014). The relative permeability estimated for several reservoir conditions is crucial information in reservoir simulation.

The elastic properties (e. g., P-wave and S-wave velocities) of CO<sub>2</sub> saturated rock sample

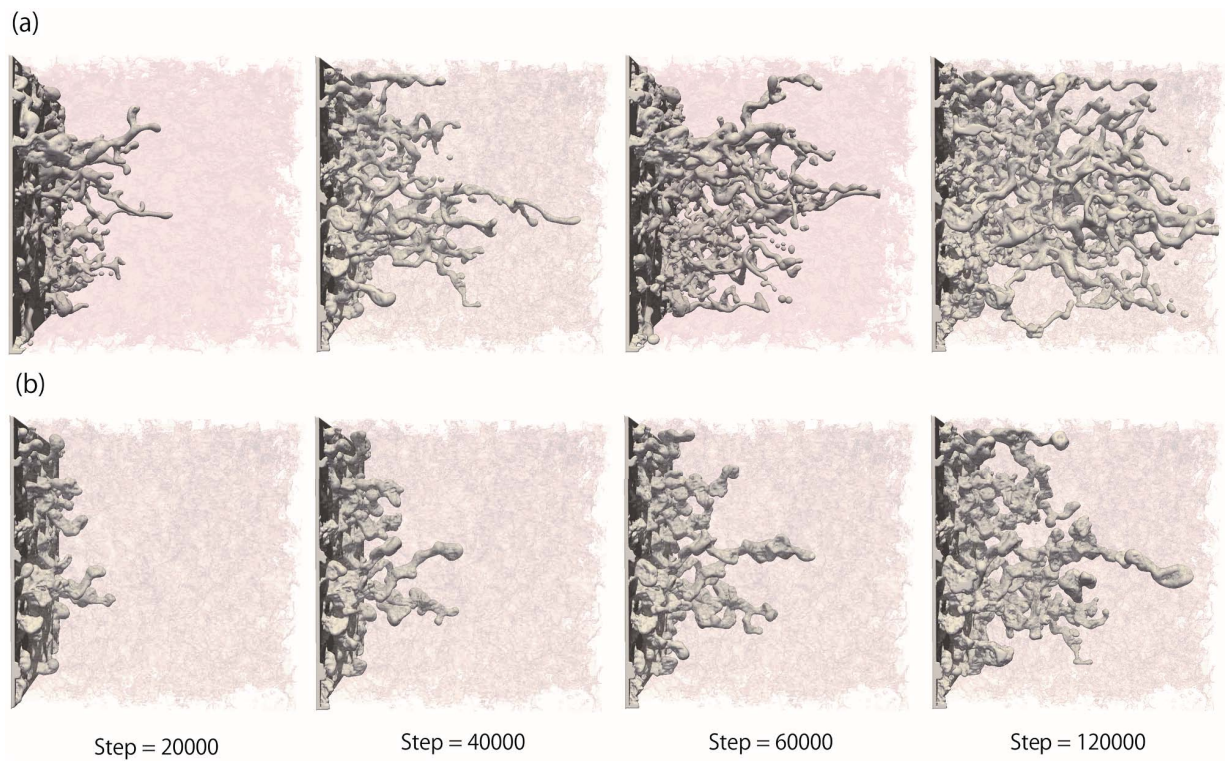


**Fig. 3.:** Non-wetting fluid invasion simulation of (a) low interfacial tension case and (b) high interfacial tension case (Jiang et al., 2014). The solid phase is shown in light gray, and the wetting fluid is transparent. The non-wetting white fluid is injected from left to right. The size of the calculated cube is 1.024 mm.

obtained via LBM (Fig. 3) are calculated by applying staggered finite-difference time-domain (FDTD) method (Saenger et al., 2011; Fig. 4). By using different frequency of source Ricker wavelet, we can estimate frequency dependence of elastic properties. Seismic velocity and quality factor can be estimated under several reservoir conditions (e.g., interfacial tension). We further obtain the relationships between seismic velocity and  $\text{CO}_2$  saturation in drainage and imbibition processes.

### Mineral precipitation modeling: Time-evolution of hydrological and elastic properties

In CCS project, the injected  $\text{CO}_2$  would be precipitated. The carbonate precipitation process is represented as a two-component system of  $\text{Ca}^{2+}$  and  $\text{CO}_3^{2-}$ . The rate of precipitation is controlled

by both changes in  $\text{Ca}^{2+}$  and  $\text{CO}_3^{2-}$  concentration in the fluid. Here, considering the equilibrium conditions, we only calculate one-component fluid with calcite for convenience (Yoo et al., 2013; Jiang and Tsuji, in revision). The calcite deposition within the pore space is calculated by using an advection–reaction formulation solved by finite volume method (FVM); we model the precipitated rock by transferring the fluid node to solid node according to the calcium concentration level. The clogging model updates the solid phase according to precipitation process and consequently changes the geometry and porosity of the sample rock. Then fluid solver is called to recalculate the flow field based on the evolved pore microstructures. Our calculation shows that deposition location depends on not only the fluid velocity field but also the rock structure. To validate our method, the carbonate precipitation simulation is carried out on a beads pack model and compared with laboratory experiment (Yoo et al.

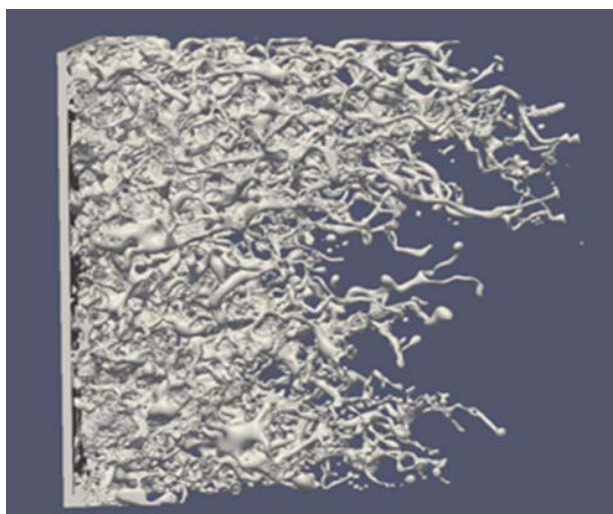


**Fig. 2.:** Example of  $\text{CO}_2$  behavior within pore space of Berea sandstone using two-phase lattice Boltzmann method. The left is inflow side. White indicates the injected  $\text{CO}_2$ . This grid size is  $1000 \times 1000 \times 1000$ .

2013). Since the simulation results are in consistent well with the experiment data, our method can simulate realistic mineralization process.

The calculated permeability variation due to the carbonate precipitation demonstrates that evolution of pore structure significantly influences the absolute permeability, while it only affects the relative permeability of non-wetting phase at low water saturation conditions. Because the non-wetting phase occupies most of the pore spaces at low wetting saturation conditions, the movement of non-wetting fluid is suppressed due to the increased capillary pressure associated with mineralization. Whereas, for high wetting saturation conditions, the relative permeability is less influenced because the non-wetting fluid inside the pore turns to separated droplets and it is possible for those droplets to pass the pore throat. These observations can be used in the long-term reservoir simulation to estimate future  $\text{CO}_2$  behaviors.

The elastic properties obtained via FDTD to the mineralized digital rock samples demonstrate that elastic properties are much influenced by the mineralization features. The relationship between seismic velocity and porosity derived from our mineralization simulation is different from that

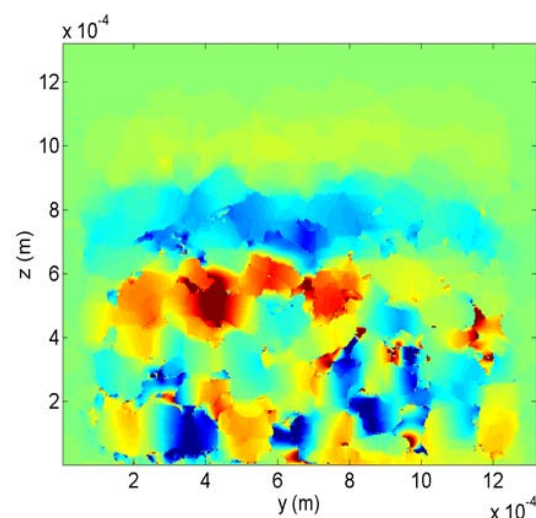


**Fig. 4.:** Elastic deformation of the LBM-derived  $\text{CO}_2$  saturated rock (Fig. 3). Elastic wave propagates from bottom to top. Color shows the velocity distribution.

derived from other mineralization methods (i. e., CT threshold adjacent method; Jiang and Tsuji, in revision). This information related to the time-evolution of elastic properties can be used in geophysical monitoring for the injected  $\text{CO}_2$ .

## Acknowledgement

I worked this study with Drs. F. Jiang and T. Ikeda. We gratefully acknowledge the support of the I2CNER, sponsored by the World Premier International Research Center Initiative (WPI), MEXT, Japan.

## References

- Jiang, F., T. Tsuji, and C. Hu (2014), Elucidating the role of interfacial tension for hydrological properties of two-phase flow in natural sandstone by an improved lattice Boltzmann method, *Transport in Porous Media*, doi:10.1007/s11242-014-0329-0.
- Jiang, F., and T. Tsuji (2014), Evolution of Pore geometry and Relative Permeability due to Carbonate Precipitation in Porous Media, *Physical Review E*, in moderate revision.

- Saenger, E.H., F. Enzmann, Y. Keehm, H. Steeb (2011), Digital rock physics: Effect of fluid viscosity on effective elastic properties, *Journal of Applied Geophysics*, 74, 236-241.
- Tölke, J., et al. (2006), An adaptive scheme using hierarchical grids for lattice Boltzmann multi-phase flow simulations, *Computers & Fluids*, 35, 820-830.
- Tölke, J. and M. Krafczyk (2008), Tera FLOP computing on a desktop PC with GPUs for 3D CFD, *International Journal of Computational Fluid Dynamics*, 22, 443-456.
- Tsuji, T., and G. Iturrino (2008), Velocity-porosity relationships of oceanic basalt from eastern flank of the Juan de Fuca ridge: The effect of crack closure on seismic velocity, *Exploration Geophysics*, 39, 41-51.
- Tsuji, T. et al. (2011), In situ stress state from walkaround VSP anisotropy in the Kumano basin southeast of the Kii Peninsula, Japan, *Geochem. Geophys. Geosyst.*, 12, Q0AD19, doi:10.1029/2011GC003583.
- Tsuji, T., H. Yamabe, T. Matsuoka (2012), LBM simulation for CO<sub>2</sub> saturation monitoring from elastic velocity and resistivity: Migration of supercritical CO<sub>2</sub> in porous media under several PT conditions, AGU fall meeting, GC51A-1176.
- Tsuji, T., R. Kamei, and G. Pratt, (2014), Pore pressure distribution of a mega-splay fault system in the Nankai Trough subduction zone: Insight into up-dip extent of the seismogenic zone, *Earth and Planetary Science Letters*, 396, 165-178, doi:10.1016/j.epsl.2014.04.011.
- Yoo, S.Y., et al. (2013), A geochemical clogging model with carbonate precipitation rates under hydrothermal conditions, *Applied Geochemistry*, 30, 67-74.

# Scientific Programme

## GeoMod2014 - Conference Outline

Time	31. August	1. September	2. September	3. September
08:45 - 09:00	-	Welcome	-	-
09:00 - 11:00	-	(Seismo-)tectonics (orals)	Volcanism and Volcanotectonics (orals)	Rheology (orals)
11:00 - 13:00	-	(Seismo-)tectonics (posters)	Volcanism and Volcanotectonics (poster)	Rheology (poster)
13:00 - 14:00	-	Lunch break	Lunch break	Lunch break
14:00 - 16:00	-	Tectonics and Surface processes (orals)	Geodynamics (orals)	Fluids and Deformations (orals)
16:00 - 18:00	-	Tectonics and Surface processes (poster)	Geodynamics (posters)	Fluids and Deformations (poster)
18:00 - 21:00	Ice Breaker Party	-	-	-
19:00 - 22:00	-	-	Joint Conference Dinner	-

**GeoMod2014 - Short course on "Constitutive Laws: from Observation to Implementation in Models"** by Onno Oncken, Mathias Rosenau, Fabio Corbi, Georg Dresen Erik Rybacki, Stephan Sobolev, and Sascha Brune  
 Thursday 4 September: 09:00 - 18:00  
 Friday 5 September: 09:00 - 14:00

**GeoMod2014 - Hands-on tutorial on "ASPECT: a next-generation geodynamic modelling software"** by Anne Glerum and Juliane Dannberg  
 Thursday 4 September: 09:00 - 18:00: Tutorial  
 Friday 5 September: 09:00 - 18:00: ASPECT Strategy Workshop (for Advanced Users) - voluntary

## GeoMod2014 Conference Programme (31 August - 3 September)

### Sunday 31 August 2014

18:00 - 21:00: Ice Breaker Party at the 'Theaterschiff Potsdam' (Schiffbauergasse 9b, 14467 Potsdam)

### Monday 1 September 2014

08:45 - 09:00: Welcome by Prof. Dr. Dr. h.c. Reinhard Hüttl and Prof. Dr. Onno Oncken

09:00 - 11:00: (Seismo-)tectonics Orals (chairs: B. Kaus, O. Oncken)

- 09:00 - 09:30: **Kelin Wang:** *Thermal Expressions of Stick-slip and Creeping Subduction Megathrusts* (keynote)
- 09:30 - 10:00: **Bertrand Maillot:** *The long-term Evolution of Fold-and-Thrust Belts: Consistency of Numerical Approaches and Physical Experiments* (keynote)
- 10:00 - 10:20: **Tasca Santimano et al.:** *Smart or Beautiful? Accretionary wedge evolution seen as a competition between minimum work and critical taper*
- 10:20 - 10:40: **Lorenzo Bonini et al.:** *The role of pre-existing frictional weaknesses on the propagation of extensional faults*
- 10:40 - 11:00: **Ylona van Dinther et al.:** *Seismo-thermo-mechanical modeling of subduction zone seismicity*

11:00 - 13:00: (Seismo-)tectonics Posters (chairs: B. Kaus, O. Oncken)

13:00 - 14:00: Lunch break

14:00 - 16:00: Tectonics and Surface processes Orals (chairs: F. Graveleau, N. Hovius)

- 14:00 - 14:30: **Ritske Huisman:** *Interaction and feedback between surface processes and mountain building* (keynote)
- 14:30 - 15:00: **Stéphane Dominguez:** *Joint analogue modelling of marine and terrestrial geological processes: state of the art and new developments* (keynote)
- 15:00 - 15:15: **Utsav Mannu et al.:** *Dynamic Modelling of Accretionary Prisms and Stratigraphy of Forearc basins*
- 15:15 - 15:30: **Karen Leever:** *3D Analogue Modelling of the Effect of Fan Sedimentation on Accretionary Wedge Dynamics – the Magdalena Fan case, South Caribbean Margin, Colombia*
- 15:30 - 15:45: **Frank Zwaan, Guido Schreurs:** *4D Transfer Zone Modeling in Continental Rift Systems*
- 15:45 - 16:00: **Sergei Medvedev, Ebbe H. Hartz:** *Evolution of topography of post-Devonian Scandinavia: Effects and rates of erosion*

16:00 - 18:00: Tectonics and Surface processes Posters (chairs: F. Graveleau, N. Hovius)

**Tuesday 2 September 2014****09:00 - 11:00: Volcanism and Volcanotectonics Orals (chairs: O. Galland, E. Holohan)**

- 09:00 - 09:30: **Rikke Pedersen**: *Surface deformation simulations of volcanic and tectonic processes in Iceland* (keynote)
- 09:30 - 10:00: **Olivier Roche**, Yarko Niño: *Mechanisms of entrainment of a granular substrate by pyroclastic density currents: insights from laboratory experiments and models, and implications for flow dynamics* (keynote)
- 10:00 - 10:15: **Rosanne Heistek** et al.: *Temporal changes in mantle wedge geometry and magma generation processes in the Central Andes: towards linking petrological data to thermomechanical models*
- 10:15 - 10:30: **Francesco Maccaferri** et al.: *The gravitational unloading due to rift depression: A mechanism for the formation of off-rift volcanoes in (continental) rift zones*
- 10:30 - 10:45: **Lola Chanceaux**, Thierry Menand: *Solidification effects on sill formation: an experimental approach*
- 10:45 - 11:00: Max Gallagher, **Ben Kennedy** et al.: *Megatsunami generation from caldera subsidence*

**11:00 - 13:00: Volcanism and Volcanotectonics Posters (chairs: O. Galland, E. Holohan)****13:00 - 14:00: Lunch break****14:00 - 16:00: Geodynamics Orals (chairs: F. Funiciello, S. Sobolev)**

- 14:00 - 14:30: **Anne Davaille**: *Plumes to Plate Tectonics: Insights from Laboratory Experiments* (keynote)
- 14:30 - 15:00: **Bernhard Steinberger** et al.: *On the relation between plate tectonics, large-scale mantle flow and mantle plumes: Some recent results and many open questions* (keynote)
- 15:00 - 15:15: **Paul J. Tackley** et al.: *Influence of Melting on the Long-Term Thermo-Chemical Evolution of Earth's Deep Mantle*
- 15:15 - 15:30: **Maria V. Chertova** et al.: *3-D numerical modeling of subduction evolution of the western Mediterranean region*
- 15:30 - 15:45: Tobias Baumann, **Boris Kaus**, A. Popov: *Constraining the rheology of the lithosphere through geodynamic inverse modelling*
- 15:45 - 16:00: **Elisa Calignano** et al.: *Strain localization during compression of a laterally heterogeneous lithosphere*

**16:00 - 18:00: Geodynamics Posters (chairs: F. Funiciello, S. Sobolev),  
Methods and Materials Posters (chairs: M. Frehner, M. Rosenau)****19:00 - 22:00 Joint conference dinner in Potsdam on the ship 'Belvedere' (Lange  
Brücke 6, 14467 Potsdam)**



**Wednesday 3 September 2014****09:00 - 11:00: Rheology Orals (chairs: G. Dresen, H. Sone)**

- 09:00 - 09:30: **Yuri Fialko**: *Numerical models of ductile roots of mature strike-slip faults* (keynote)
- 09:30 - 10:00: **Laurent Montési**: *Localization processes on Earth, Mars, and Venus* (keynote)
- 10:00 - 10:20: **Suzon Jammes et al.**: *Localization of deformation in a polymineralic material*
- 10:20 - 10:40: **Sebastian P. Müller et al.**: *Rheology of bubble- and crystal-bearing magma: new analogue experimental data and an effective-medium model*
- 10:40 - 11:00: **Maria A. Nikolinakou et al.**: *Modeling stress evolution around a rising salt diapir*

**11:00 - 13:00: Rheology Posters (chairs: G. Dresen, H. Sone)****13:00 - 14:00: Lunch break****14:00 - 16:00: Fluids and Deformations Orals (chairs: S. Miller, M. Moreno)**

- 14:00 - 14:30: **Boris Galvan et al.**: *Towards a general simulation tool for complex fluid-rock lithospheric processes: merging pre-processing, processing and post-processing in state-of-the-art computational devices* (keynote)
- 14:30 - 15:00: **Takeshi Tsuji**: *Digital rock physics: Insight into fluid flow and elastic deformation of porous media* (keynote)
- 15:00 - 15:15: **Thomas Heinze et al.**: *Numerical Modelling of earthquake swarms in the Vogtland / West-Bohemia*
- 15:15 - 15:30: **Samuel Angiboust et al.**: *Effect of Fluid Circulation on Intermediate-Depths Subduction Dynamics: From Field Observations to Numerical Modelling*
- 15:30 - 15:45: **Magdalena Scheck-Wenderoth, Judith Sippel et al.**: *Heat transport mechanisms at different scales – a 3D modelling workflow*
- 15:45 - 16:00: **Antoine Jacquey et al.**: *Modelling of fractured reservoirs: Fluid-rock interactions within fault domains*

**16:00 - 18:00: Fluids and deformations Posters (chairs: S. Miller, M. Moreno)**

The posters will be presented during the entire conference. Each poster session starts with a 1-2 min. short presentation of all participating posters.

## GeoMod2014 - Short course on "Constitutive Laws: from Observation to Implementation in Models"

### Thursday 4 September 2014

#### Morning Session: Onno Oncken, Mathias Rosenau, and Fabio Corbi

- 09:00 - 10:00: **Onno Oncken:** Observing deformation kinematics and localization: Observations from the field, geophysical imaging, and geodetic monitoring
- 10:00 - 10:15: Coffee Break
- 10:15 - 11:00: **Mathias Rosenau:** Rheology of rock analogues 1: Elastoplasticity and its application in seismotectonic simulation
- 11:00 - 11:15: Coffee Break
- 11:15 - 12:00: **Fabio Corbi:** Rheology of rock analogues 2: Viscoelasticity and its application in seismotectonic simulation
- 12:00 - 13:00: **Visit to the GFZ Analogue Lab**

#### 13:00 - 14:00: Lunch break

#### Afternoon Session: Georg Dresen and Erik Rybackii

- 14:00 - 15:15: Rheology of the lower crust : Reconciling laboratory data and field observations
- 15:15 - 15:30: Coffee Break
- 15:30 - 16:45: **Visit to the GFZ rock mechanics lab**
- 16:45 - 17:00: Coffee Break
- 17:00 - 18:00: Rock fracture processes and stick slip sliding –What do we learn from analyzing nanofemto seismicity?

### Friday 5 September 2014

#### Morning Session: Stephan Sobolev and Sascha Brune

- 09:00 - 10:00: **Stephan Sobolev:** Rheology and geodynamic modeling: key controls in plate tectonics and beyond
- 10:00 - 10:15: Coffee Break
- 10:15 - 11:30: **Sascha Brune:** Rock rheology in numerical models: PC exercises and application to rift dynamics
- 11:30 - 11:45: Coffee Break
- 11:45 - 12:30: **Stephan Sobolev:** Rheology and cross-scale modeling: towards understanding of great earthquakes
- 12:30 - 13:00: Discussion

#### 13:00 - 14:00: Lunch and end of the short course

## **GeoMod2014 – Hands-on tutorial on "ASPECT: a next-generation geodynamic modelling software" by Anne Glerum and Juliane Dannberg**

### **Thursday 4 September 2014**

#### **08:30 - 9:00: Registration**

- 09:00 - 10:00: **Tutorial 1:** First Steps – Compiling and Running ASPECT, **Lecture:** How to run and visualize simple models
- 10:00 - 11:15: **Lecture** ASPECT – A next-generation geodynamic modelling software, **Tutorial 2:** Convection in a 2D box
- 11:15 - 11:30: Coffee Break
- 11:30 - 13:00: **Tutorial 3:** Using the adaptive mesh refinement and spherical shell geometry **Lecture:** How to run and visualize simple models

#### **13:00 - 14:00: Lunch break**

- 14:00 - 15:15: **Tutorial 4:** Using the adaptive mesh refinement and spherical shell geometry and using the function parser
- 15:15 - 15:30: Coffee Break
- 15:30 - 17:00: **Tutorial 5:** Averaging at the example of subduction and using a “sticky air” layer
- 17:00 - 18:00: **Voluntary:** Installing ASPECT on personal computers

**18:30: Joint Dinner (to be payed by the participants)**

### **Friday 5 September 2014**

**09:00 - 18:00: ASPECT Strategy Workshop for Advanced Users: Perspectives for Modelling with ASPECT**

## Index

- Abid, M., 101  
Acocella, V., 177, 206, 231  
Adamuszek, M., 352  
Agard, P., 393  
Ahmadzadeh, M. I., 3  
Aller, A. L., 275  
Almeida, J., 144  
Alonso-Henar, J., 62  
Alvarez-Gomez, J. A., 62  
Alves da Silva, F. C., 67  
Amirzada, Z., 424, 457  
Angiboust, S., 393  
Artemieva, I. M., 235  
Averbuch, O., 112
- Babeyko, A., 149  
Badmus, B. S., 395, 396  
Bagge, M., 7  
Barantseva, O., 235  
Barata, F., 144  
Barrientos-García, B., 459  
Basili, R., 9  
Battaglia, M., 196  
Baumann, T., 237  
Bedford, J., 26  
Blöcher, G., 407  
Blanco, A., 67  
Bonini, L., 9  
Brandes, C., 71  
Brandmeier, M., 188  
Brizzi, S., 14  
Broichhausen, H., 452  
Brune, S., 239, 242  
Buiten, S., 246, 334  
Bull, A. L., 313  
Bulois, C., 181  
Burchardt, S., 181  
Burov, E., 393  
Burrato, P., 9
- Burtin, A., 424
- Cabral, F. R., 285  
Cacace, M., 247, 407, 412  
Cailleau, B., 211  
Calignano, E., 249  
Carmona, A., 75  
Carvalho, B., 144  
Cavozzi, C., 298  
Cerca, C., 459  
Cerca, M., 108  
Chanceaux, L., 172  
Chatton, M., 114  
Chen, Z., 266  
Chertova, M. V., 254  
Cherubini, Y., 412  
Clavera-Gispert, R., 75, 80  
Cloetingh, S., 336, 387  
Cnudde, V., 217  
Contreras, J., 299  
Cook, K., 84  
Corbi, F., 14, 37, 177, 430  
Corti, G., 108, 428  
Cruden, A. R., 17, 266
- Dabrowski, M., 294, 352, 355  
Dalguer, L. A., 22, 52  
Dannberg, J., 259, 320  
Davaille, A., 261  
Davies, T., 178  
De Guidi, G., 226  
Di Giuseppe, E., 430  
Dominguez, S., 85, 114  
Dotare, T., 434  
Duarte, J. C., 144, 266  
Dumazer, G., 439  
Dumke, A., 211  
Dutta, U., 269
- Egglseder, M., 17

- Eken, T., 424  
Ellis, J. F., 452  
Endo, I., 448
- Faleide, J. I., 140, 281  
Fialko, Y., 358  
Flemings, P. B., 376  
Fomin, I., 329  
Fraters, M., 272  
Frehner, M., 89, 95  
Freytmuth, H., 188  
Fritzell, E. H., 275  
Fuente, J. A. M. de la, 75  
Funicello, F., 14, 37, 430
- Gärtner-Roer, I., 95  
Gabrielsen, R. H., 140  
Gaina, C., 313  
Gallagher, M., 178  
Galland, O., 181, 185, 439  
Galvan, B., 397, 401, 404  
Gao, X., 56  
Garcia-Sancho, C., 363  
Gassmoeller, R., 320  
Geenen, T., 254  
Gerya, T., 22, 37, 52, 121, 131, 285, 289, 336  
Ghani, H., 101  
Ghazian, R. K., 246  
Gisler, G., 185  
Glerum, A., 272, 331  
Gloaguen, R., 149  
Gomes, C. J. S., 448  
Gomez, C., 178  
Gover, R., 363  
Gracia-Marroquín, D., 108  
Gratacos, O., 75, 80  
Graveleau, F., 84, 112, 114  
Großmann, J., 452  
Guéguen, Y., 159  
Gueydan, F., 368  
Guillou-Frottier, L., 289  
Görz, I., 443
- Hallot, E., 181  
Hamidi, S., 397, 401, 404  
Hampel, A., 7, 347  
Hardy, S., 75  
Hartz, E. H., 136
- Haug, Ø. T., 185, 424, 457  
Hayman, N. W., 324  
Heine, C., 239  
Heinze, T., 397, 401, 404  
Heistek, R., 188  
Herceg, M., 235  
Herrendörfer, R., 22  
Herwegh, M., 381  
Hillebrand, B., 331  
Hinsbergen, D. J. J. van den, 254  
Holohan, E. P., 191, 211, 217, 439  
Hori, T., 434  
Hovius, N., 84  
Hudec, M. R., 376  
Huismans, R. S., 116  
Hussain, H., 101
- Iandelli, I., 428  
Imposa, S., 226
- Jacquey, A., 407  
Jammes, S., 365  
Jansen, G., 397  
Javed, E., 101  
Johansen, E., 117  
Jolivet, L., 289
- Kaban, M. K., 304, 387  
Kagan, A. I., 49  
Kaiser, B. O., 412  
Karatun, L., 276  
Karrech, A., 381  
Kastelic, V., 9  
Kaus, B., 237, 308  
Keir, D., 206  
Kelly, B. F. J., 153  
Kennedy, B., 178  
Kervyn, M., 217  
Khan, I., 101  
Khatami, M., 397  
Klemann, V., 278  
Klitzke, P., 281  
Kullberg, C., 144
- La Marra, D., 196, 231  
Lavier, L. L., 324, 365  
Leever, K., 117, 310, 457  
Lennox, P., 153

- Leroy, Y. M., 159  
Lewerenz, B., 412  
Li, H., 201  
Li, S., 26  
Liao, J., 121  
Ling, A. H. M., 95  
Llewellyn, E. W., 372  
Lopez-Blanco, M., 80  
Lourenço, D. L., 284, 329
- Maccaferri, F., 177, 206  
Mader, H. M., 372  
Mai, P. M., 52  
Maillot, B., 29, 159  
Malavieille, J., 114  
Malik, A., 101  
Mandal, N., 269  
Manighetti, I., 114  
Mannu, U., 131  
Mares, C., 459  
Marques, F. O., 285  
Martinec, Z., 278  
Martinez-Diaz, J. J., 62  
Massmeyer, A., 430  
Matenco, L., 336  
May, D. A., 285  
Maystrenko, Y. P., 412  
Medvedev, S., 136  
Melnick, D., 26  
Menand, T., 172  
Menant, A., 289  
Miller, S., 397, 401, 404  
Miraj, M. A. F., 140  
Montesi, L. G. J., 368  
Mooney, W. D., 387  
Moreno, M., 26  
Moroni, M., 14  
Mourgues, R., 181  
Mueller, S. P., 372  
Mukherjee, S., 43  
Muldashev, I. A., 33  
Mulyukova, E., 294, 320  
Musiol, S., 211
- Nadimi, A., 318  
Nakawaga, T., 329  
Naliboff, J., 334
- Nestola, Y., 298  
Neumann, F., 299  
Niño, Y., 221  
Nikolinakou, M. A., 376  
Noack, V., 412
- Offler, R., 153  
Oncken, O., 26, 39, 310, 457  
Ouzgaït, M., 112
- Pérez-gussinyé, M., 239  
Palano, M., 226  
Parang, S., 300  
Pascal, C., 140  
Pauwels, E., 217  
Pearson, D. G., 342  
Pedersen, R., 214  
Pellerin, J., 443  
Peters, M., 381  
Petit, C., 114  
Petrinin, A. G., 304  
Pinel, V., 177  
Popov, A., 237, 308  
Poppe, S., 217  
Portillo-Pineda, R., 108  
Poulet, T., 381  
Pranger, C., 36, 37  
Pusok, A. E., 308  
Pysklywec, R., 276
- Quinion, A., 112  
Quinteros, J., 340
- Rahimi, H., 3  
Reber, J. E., 365  
Regenauer-Lieb, K., 381  
Ritter, M. C., 310  
Rivalta, E., 177, 206, 231  
Roche, O., 221  
Rodrigues, B. A., 448  
Rosas, F. M., 144  
Rosenau, M., 26, 39, 310, 424, 457  
Ruch, J., 231
- Sakaguchi, H., 434  
Santimano, T., 39  
Santimano, T. N., 430  
Sarkar, S., 269

- Sarocchi, D., 459  
Sasgen, I., 278  
Schöpfer, M. P. J., 191  
Scheck-Wenderoth, M., 247, 281, 407, 412  
Schellart, W. P., 266  
Schmalholz, S., 331, 464  
Schmeling, H., 304  
Schmid, D. W., 352  
Schreurs, G., 62, 164  
Schroeder, S., 149  
Scudero, S., 226  
Sedano, L. A. R., 459  
Seno, S., 9  
Shephard, G. E., 275, 313  
Singh, P., 43  
Sippel, J., 281, 412  
Sobolev, S. V., 33, 149, 239, 259, 294, 320, 340  
Sobouti, F., 3  
Sohrabi, A., 318  
Sokoutis, D., 249  
Sone, H., 385  
Spakman, W., 36, 254, 272, 331, 334  
Steinberger, B., 294, 304, 320  
Sternai, P., 289  
Storti, F., 298  
Strak, V., 114  
Strasser, M., 131  
Sudhaus, H., 191  
Suppe, J., 84  
Suzuki, N., 46  
Svartman Dias, A. E., 324
- Tackley, P. J., 284, 329  
Tatarinov, V. N., 49  
Tatarinova, T. A., 49  
Terrinha, P., 144  
Tesauro, M., 278, 363, 387  
Tetreault, J., 246  
Thieulot, C., 36, 272, 276, 331, 334  
Thybo, H., 235  
Tolosana-Delgado, R., 80  
Tolson, G., 299  
Tomás, R., 144  
Torsvik, T., 331  
Toscani, G., 9  
Tripanera, D., 231  
Truby, J. M., 372
- Träger, F., 443  
Tsuji, T., 417  
Turowski, J., 84  
Tutu, A. O., 332  
Tympel, J., 149
- Ueda, K., 131
- Valensise, G., 9  
van den Berg, A., 36  
van den Berg, A. P., 254  
van Dinther, Y., 22, 37, 52  
van Gasselt, S., 211  
van Hunen, J., 342  
van Zelst, I., 334  
Vazquez, A., 299  
Vendeville, B., 112  
Veveakis, M., 381  
Vogt, K., 336  
von Tscharner, M., 464
- Wörner, G., 188  
Walsh, J. J., 191  
Walter, M., 340  
Walter, T. R., 191, 211  
Wang, H., 342  
Wang, K., 56  
Warners-Ruckstuhl, K. N., 363  
Watanabe, K., 201  
Willett, S. D., 131  
Williams, D. A., 211  
Willingshofer, E., 249  
Winsemann, J., 71  
Wolff, S., 393
- Yamada, Y., 434  
Yamato, P., 393  
Yan, J., 153  
Yassaghi, A., 467  
Yonezu, K., 201  
Yuan, X., 159
- Zafar, M., 101  
Zehner, B., 443  
Zeoli, A., 428  
Zeumann, S., 347  
Zhu, G., 285  
Zwaan, F., 164